sustainability

MDPI

Article

Towards Sustainable Electricity for All: Techno-Economic Analysis of Conventional Low-Voltage-to-Microgrid Conversion

Frimpong Kyeremeh [1,2,*], Dennis Acheampong [3], Zhi Fang [1], Feng Liu [1] and Forson Peprah [3]

[1] College of Electrical Engineering and Control Sciences, Nanjing Tech University, No. 30 South Puzhu Road, Pukou District, Nanjing 211800, China; myfz@263.net (Z.F.); f.liu_1@hotmail.com (L.F.)
[2] Electrical & Electronic Engineering Department, Faculty of Engineering, Sunyani Technical University, Sunyani P.O. Box 206, Ghana
[3] Regional Centre for Excellence in Energy and Environmental Sustainability, School of Engineering, University of Energy and Natural Resources (UENR), Sunyani P.O. Box 214, Ghana; dennisacheamp@gmail.com (D.A.); pepraforson@yahoo.com (F.P.)
* Correspondence: frimpong.kyeremeh@stu.edu.gh

Abstract: Ghana's electricity grid remains heavily fossil-fuel dependent (69%), resulting in high costs and unstable low-voltage (LV) networks, exacerbating supply shortages. This study evaluates the technical and economic feasibility of converting the Obaa-Yaa LV substation in Drobo, Ghana, into a solar-powered microgrid. Using the forward–backward method for technical analysis and financial metrics (NPV, IRR, DPP, and PI), the results show that rooftop solar on seven households generates 676,742 kWh annually—exceeding local demand by 115.8 kW—with no voltage violations (240 V ± 6%) and minimal losses (9.24 kW). Economic viability is demonstrated via an NPV of GHS 2.1M, IRR of 17%, and a 10-year payback. The findings underscore solar microgrids as a pragmatic solution for Ghana's energy challenges, urging policymakers to incentivize decentralized renewable systems.

Keywords: sustainable energy; low-voltage network; techno-economic analysis; microgrid

check for updates

Academic Editors: Carlos Vargas-Salgado and Jesus Aguila-Leon

Received: 28 April 2025
Revised: 23 May 2025
Accepted: 27 May 2025
Published: 4 June 2025

Citation: Kyeremeh, F.; Acheampong, D.; Fang, Z.; Liu, F.; Peprah, F. Towards Sustainable Electricity for All: Techno-Economic Analysis of Conventional Low-Voltage-to-Microgrid Conversion. *Sustainability* **2025**, *17*, 5178. https://doi.org/10.3390/su17115178

Copyright: © 2025 by the authors. Licensee MDPI, Basel, Switzerland. This article is an open access article distributed under the terms and conditions of the Creative Commons Attribution (CC BY) license (https://creativecommons.org/licenses/by/4.0/).

1. Introduction

1.1. Rationale of This Study

Globally, there has been a significant transformation in the energy landscape in recent years due to the increasing concerns over climate change and the need for sustainable energy solutions. Conventional electricity generation heavily relies on fossil fuels, which heavily contribute to greenhouse gas emissions to the environment. As a result, there is a growing urgency to transition towards sustainable energy (RE) sources to mitigate these negative impacts [1,2]. Low-voltage (LV) systems are crucial in supplying electricity to end-users, thus residential, commercial, and industrial in the electricity value chain. The LV networks are traditionally powered by centralised generation sources, often connected to the primary grid. Solar photovoltaic (PV) electricity grid integration and microgrid development have gained considerable attention in modern times due to the abundance of the resources and the per-watt cost of the technology [3,4]. Microgrids, modular versions of conventional distribution systems but with renewable sources powering them, have emerged as an innovative solution for achieving energy independence and increasing the resilience of local power supply. Microgrids can work as a standalone network or be connected to the existing grid network, providing a reliable and sustainable electricity supply to specific areas or communities [3,5–8]. Some researchers argue that the proliferation of REs on

the distribution network causes power quality problems; other authors refute this claim that overvoltage and network losses are minimised in the network [1,9–11]. While several researchers have written on the technical aspects of microgrids, others have written on the economic side. Whereas studies in ref. [12] analysed the economics of medium-voltage microgrid conversion, ref. [13] evaluated the economics of three types of prosumers in a microgrid.

It is obvious that microgrids are becoming the solution for power system sustainability; since fossil fuel sources primarily power traditional grids, it which threatens the power sector sustainability, and therefore, the need to shift to REs. The benefits of microgrids include reliability in electricity supply, reduction in greenhouse gas emissions, and enhancement of energy efficiency.

The electricity situation in Ghana is not different from the global trend. Demand keeps increasing, while primary input supply to power plants is predominantly from fossil fuel sources. At present, the fossil fuel-based generation portfolio is about 69% of the total electricity supply in the country. The unreliability in fuel supply and associated high cost of thermal plant electricity generation result in frequent power outages and load shedding due to demand–supply imbalances and the grid infrastructure limitations. This adversely affects the quality of life and economic activities in Ghana, particularly in rural areas. Furthermore, the unreliable power supply in Ghana undermines sole reliance on the national grid [14].

Therefore, there is a need to explore the possibility of converting existing LV grids into a solar-powered microgrid which can operate independently or with the main grid (on-grid microgrid). Owing to the above, this study therefore aims to conduct a comprehensive technical and economic analysis of converting low-voltage distribution networks into solar-powered microgrids for achieving power sector sustainability.

1.2. Novelty and Contribution

This study introduces a novel approach by converting a low-voltage fossil-fuel-dependent grid in Ghana (Obaa-Yaa substation in the Drobo district) into a solar-powered microgrid using rooftop PV systems. Unlike prior studies that primarily analyse medium-voltage networks or standalone off-grid systems, this study integrates real-world data from an existing distribution substation severing consumers at a location of high solar resource. The study is presented into two distinct dimensions—technical and economic. The technical evaluation employs the forward–backward method implemented in Python 3.11.10 for the LV network with high R/X ratios load flow studies, and the solar PV system designs uses a GIS application and empirical power system method. The economic evaluation uses four different economic matrices (NPV, PI, DPP, and IRR) to justify the traditional LV grid-to-solar-powered microgrid conversion based on the prevailing economic conditions in Ghana. The outcome of this case study presents a model for similar studies, globally.

1.3. Related Works

1.3.1. Electrification Challenges in Ghana

Ghana's effort to achieve 100% universal electricity is on a slow pace. At present, the access rate is 85%, while the current installed capacity is 5615 MW with peak demand of 3848 MW. This means that about 5.26 million people lack electricity in the country. Meanwhile, electricity access is a critical factor for socio-economic development, yet many rural areas in Ghana face significant challenges in accessing electricity for their communities. The existing grid infrastructure often fails to reach these remote areas, leaving them underserved or completely off-grid [2]. Without electricity, various socio-economic activities, including healthcare, education, business opportunities, and agriculture, will be hindered.

The challenges of electrification in Ghana are multifaceted. On the supply side, unreliability in fuel supply and associated high cost of thermal plant electricity generation result in frequent power outages and load shedding. This challenge is driven by demand–supply imbalances and the grid infrastructure limitations. The country's geographical layout poses challenges in extending the national grid to off-grid communities. The cost of transmission and distribution networks is the major challenge. This adversely affects the quality of life and economic activities in Ghana, particularly in rural areas [14]. Furthermore, the unreliable power supply in Ghana undermines sole reliance on the national grid [14]. However, all must have access to electricity as per the SDG goal 7 [15].

Therefore, there is a need to explore the possibility of converting existing LV grids into a solar-powered microgrid which can operate independently or with the main grid (on-grid microgrid). Solar-powered microgrids are the way to go, leveraging the abundant sun's radiant energy in the country [11]. Converting low-voltage distribution networks into solar-powered microgrids can be a viable and environmentally friendly approach to addressing the electrification gap in Ghana [1].

1.3.2. Solar-Powered Microgrids as a Solution

Solar-powered microgrids are the stop-gap solution for rural electrification in developing nations. The advantages are enormous over the traditional grid extension [16]. These microgrids combine solar PV systems including storage and intelligent energy management systems to provide localized and sustainable electricity generation and distribution. The following key aspects highlight the significance of solar-powered microgrids. (i) Solar-powered microgrids operate as a standalone system or connected to the grid network, enabling decentralized energy generation. The latter is called an on-grid microgrid. This decentralization reduces reliance on centralized power plants and transmission lines, which often struggle to reach remote areas. Solar microgrids eliminate transmission and minimize distribution losses, thereby increasing overall system efficiency [17,18]. With an on-grid microgrid and storage, the supply's reliability to consumers can be guaranteed. (ii) Ghana has an abundance of solar resources that can be harnessed to generate electricity. Solar-powered microgrids harness this renewable energy source through PV panels, converting sunlight into electricity. Microgrids use solar power to reduce carbon emissions and promote electricity sustainability [19,20]. (iii) Solar-powered microgrids offer increased energy resilience, particularly in areas prone to power outages or where the national grid is unreliable. With storage systems, any energy can be stored for future use. This forms the basis for a stand-alone system and provides several benefits, such as a stable and reliable power supply to hospitals, schools, and off-grid communities. (iv) Solar-powered microgrids can be scaled up or modified to meet growing electricity demands [12]. (v) Solar-powered microgrids enable local communities to take part in generating and managing energy. By implementing community ownership models, a sense of responsibility and ownership is cultivated. This also opens up opportunities for entrepreneurship, job creation, and economic growth within the community [21]. (vi) Solar-powered microgrids eliminate or minimize the need for extensive transmission and distribution infrastructure, reducing transmission losses and associated costs. This cost-effective approach makes solar-powered microgrids economically competitive with grid extension in remote areas.

1.3.3. Technical Considerations for Micro Grid Implementation

The deployment of solar-powered microgrids requires certain technical considerations for successful integration and maximum efficiency. The following points outline the key aspects to consider when designing and implementing a solar-powered microgrid. (i) Conducting a thorough load assessment is essential to determine the electricity de-

mand of the target community. This includes analysing existing and projected energy consumption patterns, peak load requirements, and specific energy needs for different sectors such as residential, commercial, and agricultural. Understanding the load profile helps size the solar PV system and energy storage capacity accordingly. (ii) Practical solar resources assessment is crucial during the design stage. The assessment involves irradiation measurements and shading determination. This assessment helps determine the appropriate number and orientation of PV panels, ensuring optimal solar energy capture. Solar maps have been developed for many countries to assist this assessment. Figure 1 shows the Ghana's solar map. The country receives an average of 4.4–5.6 kWh/m^2/day of solar radiation [19]. The daily radiation indicates abundant solar resources convertible to electricity in Ghana. Nevertheless, nearly only 1% is featured in the country's generation mix.

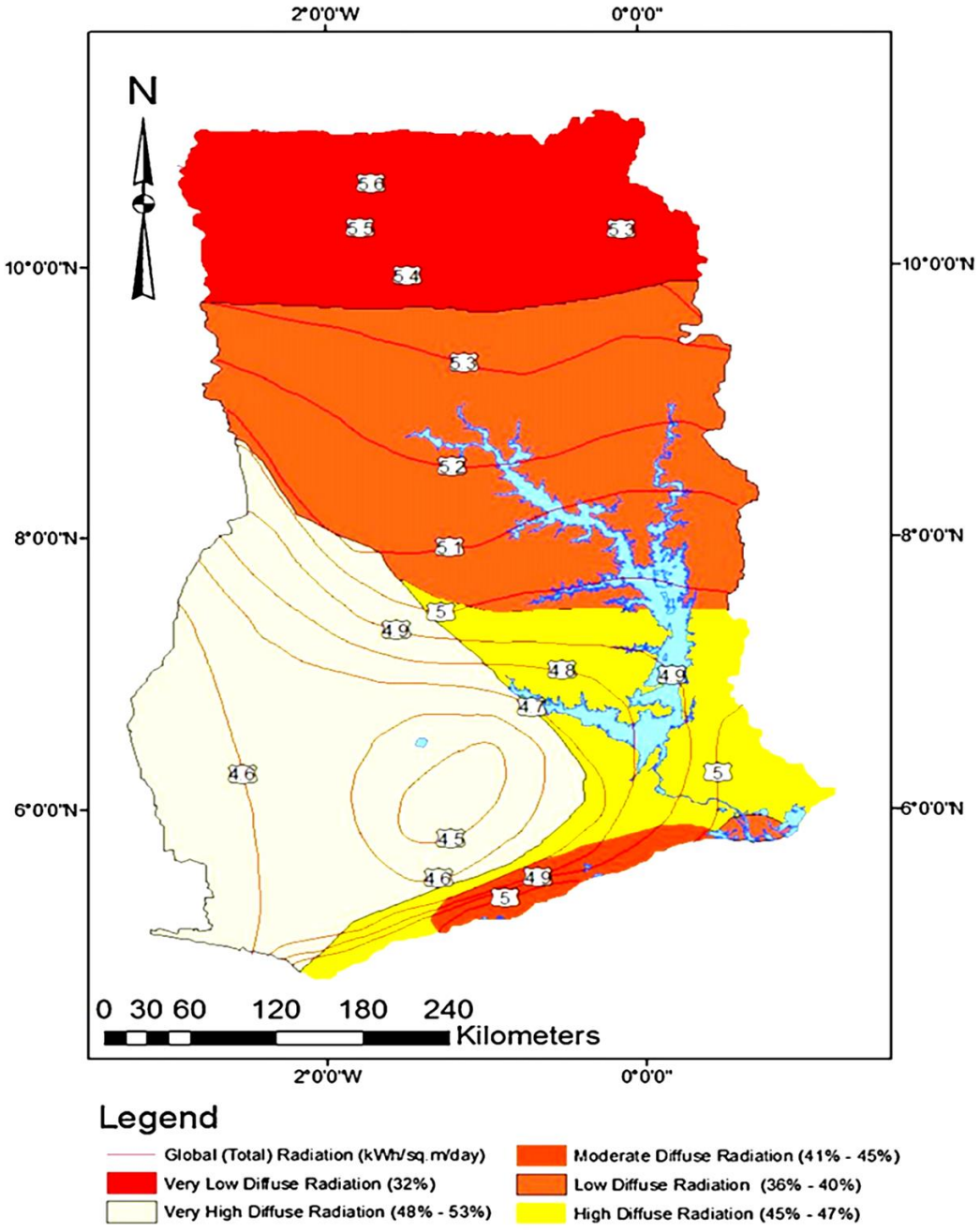


Figure 1. Solar resource distribution in Ghana [2].

The design of a solar-powered microgrid includes selecting the system components and configuring their interconnection—components like panels, batteries, inverters, cables, and energy management systems. Properly sizing and selecting these components are essential to meet the electricity demand and ensure system reliability [22]. Integrating the solar-powered microgrid with the existing low-voltage distribution network requires careful planning and coordination. It involves assessing the hosting capacity of the existing infrastructure. These include transformers, switchgear, and distribution lines. Appropriate interconnection protocols and protection mechanisms need to be established to ensure seamless and safe integration [23–25].

Maintaining system reliability is critical for uninterrupted electricity supply. Microgrids should be designed to withstand fluctuations in solar energy generation and variations in load demand. Voltage regulation mechanisms, such as voltage control devices and power quality monitoring systems, ensure stable voltage levels and protect connected appliances and equipment [3,12]. Implementing load management strategies and demand response mechanisms can enhance microgrids' reliability and efficiency. This involves optimizing electricity consumption through load shifting, load shedding, and demand-side management techniques. Smart control systems enable real-time monitoring and control of loads, ensuring efficient utilization of available energy resources [26]. Regular monitoring and maintenance are essential for the smooth operation of a solar-powered microgrid. This includes monitoring the performance of PV panels, battery health, inverter efficiency, and overall system performance. Adequate maintenance and servicing ensure maximum system efficiency, longevity, and optimal energy generation [26].

1.3.4. Power Flow Methods

Several studies underscore power flow algorithms for distribution systems [27]. The general classification of the PF algorithm is the Gauss–Seidel iterative, sequential substitution (also called the impedance method), and piecewise solution method. Among the aforementioned are the ladder iterative technique [28], backward or forward method [2,29,30], Newton–Raphson (NR) [31], and P-Q decoupled or fast decoupled method [8,11,32]. The new era in PF studies also employs the artificial intelligence theory (AIT) [33], the genetic algorithm (GA) [34], the artificial neural network (ANN) algorithm, and fuzzy logic [35]. Ref. [36] proposed graph theory-based PF algorithm, Refs. [4,37] developed models to analyse radial distribution systems [29] that had voltage-dependent loads connected to them. Ref. [38] used a linear approximation method to provide a solution to distribution networks' power flow problem. Ref. [39] applied the symmetrical components approach based on nodal admittance matrices to solve a three-phase transformer problem. Ref. [31] used CPU (complex per unit normalization) method to improve the fast-decoupled method's performance. Some considerations apply to most of these existing methods of PF studies in distribution systems (DS). Among the considerations are a high line ratio of resistance to reactance (R/X), mixing of overhead and underground sections, unbalanced phase conditions, and weak mesh topologies [29,31,36]. In addition to these considerations, three-phase transformers supply single-phase and three-phase (balanced and unbalanced) loads. Another consideration is using voltage regulators to help achieve voltage regulation under different loading conditions in DS simulations. Therefore, the NR-based PF algorithm diverges with these factors [36]. Notwithstanding the issues with most existing methods, they have unique characteristics. The Gauss–Seidel iterative method is simple and requires small memory. Conversely, its convergence is not satisfactory. High memory requirement and computational burden are the demerits of the impedance method compared to the Gauss–Seidel method. The impedance method is still the favoured method widely used in load flow calculation today due to its convergence, memory demand, and computing

speed compared to other methods [35]. The NR-based PF method suffers from the ill-conditioning problem and low convergence when applied to DSs. In an ill-conditioned system, slight variations in network parameters lead to significant changes in the system's outputs. Among the existing methods, the most effective is the fast decoupled method. It is the most straightforward and efficient method [35], but performs poorly with the distribution system [36]. The forward and backward sweep is simple and does not require a Jacobian matrix; it depends on a voltage-controlled bus. It suits small networks and online and offline problems [33,40].

The modern methods come with distinctive characteristics, but they have issues. The genetic algorithm (GA) is simple and fits offline problems. However, it requires much computational time in complex networks. It is also sensitive to controller parameters. The artificial neural network (ANN) is suitable for large-volume data sets and is best for online problems. Nevertheless, the specified input range is restricted and requires a significant computational burden. The load flow analysis of this study hinges on the forward and backward method since it is suitable for small networks and online and offline problems.

1.3.5. Economic Indices of Solar PV Projects

Conducting a comprehensive economic analysis using economic indicators is essential to assess the viability and financial sustainability of converting a low-voltage grid into a PV microgrid. Several economic and financial methods are commonly employed in evaluating the economic feasibility of such projects [2]. The following explains the significance of these economic or financial indicators: Net present value (NPV) is an economic indicator that evaluates the success of a project by comparing project's present value of cash-in and cash-out over the lifespan. The time value of money is a key measure in the method. Future cash flows are discounted to their present value, at a predetermined discount rate. If the result shows positive, the project is financially viable. If it shows negative, the project is not viable. Internal rate of return (IRR) can be used to appraise a project viability by determining a discount rate that makes the NPV zero. If the computed discount rate is higher than the initial discount rate, the project is viable, otherwise, it is not viable [13]. The indicator that expresses the ratio of cash-in to cash-out, while time value of money is considered is called the profitability index (PI). A PI more than one is desired, and this indicates financial viability of the proposed project. While a PI less than one is considered an unattractive investment. The period at which project cash inflow equals the outflows is called the payback period. This is a quick measure to know the project attractiveness. Shorter payback period is required for good investment [2].

A comparative analysis of the previous studies is presented in Table 1. It highlights key parameters, such as the voltage levels addressed, the technical methodologies employed, the economic considerations or focuses integrated within the studies, and the main limitations identified in each case. This comparative framework contextualizes the current study within the broader field and underscores its unique contributions and the specific gaps it addresses in relation to prior work.

The rest of this study is as follows: Section 2 presents the methodology used, and Section 3 presents the results and discusses them.

Table 1. A comparative table of voltage level, technical method, economic focus, and key limitations in the available literature.

Authors	Country	Voltage Level	Technical Method	Economic Focus	Key Limitation
Peprah et al. [1]	Ghana	LV	Not applicable	Prosumer economics	LV network focus and rooftop integration
Kaushal et al. [7]	India	LV	ANN-based control	Power quality economics	High R/X ratio adaptation
Asante et al. [12]	Ghana	LV	Empirical analysis for PV sizing	NPV, IRR, PI, and DPP	No load flow studies were done. Small LV network which belongs to one consumer
This Study	Ghana	LV	Forward–backward sweep, Python simulations, and empirical power system method	NPV, IRR, PI, and DPP	Leasing of the rooftops, and consumers and stakeholder acceptance Transient stability and short-circuit analysis are not considered

2. Methodology

This study's methodology is presented in this section. It includes an LV microgrid design concept and definition, load modelling and management strategy, other system modelling, load flow, case study, and solar PV microgrid assessment.

2.1. LV Microgrid Concept and Definition

The system design phase determines configuration and solar PV systems size for converting an LV grid (case study) into a solar-powered microgrid. Factors such as the available roof space, land area, solar resource availability, and electricity demand are considered in the design. Python simulations under different system configurations assess the network performance under varying conditions, including solar PVs. Critical considerations in the system design include determining the capacity and placement of solar panels and integrating the solar PV systems with the existing distribution network. Inverter selection, battery storage options, and control systems are also evaluated. The design aims to maximise solar energy generation, optimise system efficiency, and ensure seamless integration with the grid. In Figure 2, the conceptual design of the proposed LV microgrid is shown. It has a distribution transformer being supplied from an existing medium voltage (MV) network. The transformer's output is fed to an LV network that supplies several commercial and residential customers, which is called the conventional network. This conventional network is transformed into a microgrid network through solar PV plants selected at vantage points on the LV network to serve the consumers. With the PV plants on board, the network can operate in two modes: (i) independently as standalone network and, or (ii) to operate with the MV grid through the distribution transformer. Any excess energy generated after serving the consumers and storage requirements will be exported to the MV network if it operates in the latter mode. Figure 3 shows the workflow of the various subsystems. The energy management includes reactive power compensation, and grid interaction.

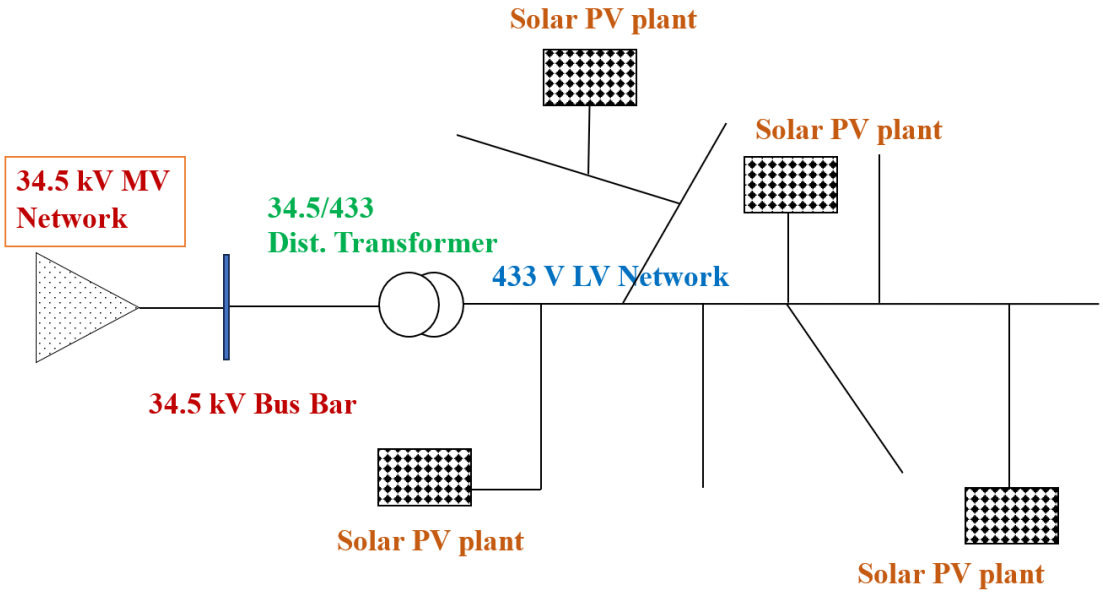


Figure 2. One-line diagram of the proposed LV microgrid.

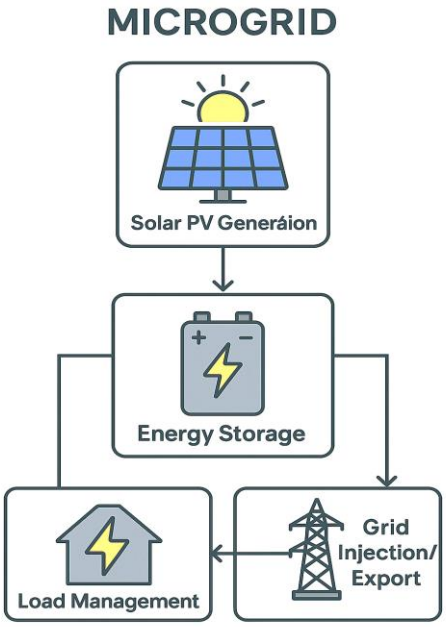


Figure 3. Operational workflow of the solar-powered microgrid, highlighting PV generation, storage dispatch, and grid interaction.

2.2. Load Model and Management Strategy

The load model in this study is three-phase unbalanced loads (P + jQ), mimicking a typical LV network. The unbalanced nature of line loading influences the system performance on node voltages and line losses. This study's load management strategy is to effectively shift consumers' peak load to daytime to utilise solar-generated electricity in the neighbourhood. This study assumes that each load operates at its maximum nameplate ratings while the PV system serves them through the microgrid. During sun hours, merit order dispatch is considered between the PV generation and storage to serve the load. These strategies also contextualise the mixed characteristics of residential and commercial loads in the area and the needed electricity to meet the demand effectively without shortages. The management strategy aims to balance electricity supply and demand, optimise energy utilisation, and ensure reliable and stable operation of the solar-powered microgrid.

2.3. Grid Impact

Integrating solar PV systems into the low-voltage distribution network may impact its stability in terms of power quality and voltage regulation. A grid stability assessment is conducted to evaluate the technical implications of the solar-powered microgrid conversion. This assessment involves analysing the hosting capacity (nodal voltages and losses) of the PV system on the existing LV network. Figure 4 shows the simplified one-line diagram of the proposed LV grid. It is made up of a medium voltage (MV) network, distribution transformer, LV lines, and loads connected at different locations. The MV network supplies the transformer at 34.5 kV, and the transformer steps down the MV voltage to 433 V to supply the load through the LV network. Due to the line impedance and current flow, there is a voltage drop between buses 1 and 2. The voltage at bus 2 will be less than at bus 1. Since the load bus is also specified in most power system studies, starting load flow analysis from the load side is convenient. Let S_{load}, P_{load} and Q_{load} be the apparent, active, and reactive powers of the load, respectively. Equation (1) describes the relationship between S_{load}, P_{load}, and Q_{load}. The current in the load is expressed as Equation (2).

$$S_{Load} = P_{Load} + jQ_{Load} \tag{1}$$

$$I_{Load} = \frac{S_{load}}{V_2} = \frac{P_{load} + Q_{load}}{V_2} \tag{2}$$

The current (I_{inj}) in the line between bus 1 and 2 will be the same as Equation (2), expressed in Equation (3) as follows:

$$I_{inj} = I_{load} = \frac{S_{inj}}{V_1} = \frac{V_1 - V_2}{Z} = \frac{P_{load} + Q_{load}}{V_2} \tag{3}$$

where the load's active power is represented by P_{Load}, its reactive power is jQ_{oad}, I_{inj} denotes the line current, V_1 and V_2 indicate the voltage at buses 1 and 2, respectively, and S_{inj} represents the apparent injection by the transformer to the line. The line's power loss and voltage drop are denoted as S_{loss}, and V_d can be expressed as Equations (4) and (5), respectively, as follows:

$$S_{Loss} = I_{inj} V_d = \left(\frac{S_{inj}}{V_1}\right)^2 Z = \left(\frac{V_1 - V_2}{Z}\right)^2 Z = \left(\frac{P_{load} + Q_{load}}{V_2}\right)^2 Z \tag{4}$$

$$\mathrm{V}_d = \mathrm{I}_{\mathrm{inj}} \cdot Z = \left(\frac{S_{inj}}{V_1}\right) Z = \left(\frac{V_1 - V_2}{Z}\right) Z = \left(\frac{P_{load} + Q_{load}}{V_2}\right) Z \tag{5}$$

Note Z = $R_i + jX_i$

A typical LV grid has more nodes and sections than shown in Figure 2. From Equation (3), the S_{inj} injected can be expressed in Equation (6). In a typical LV network, the apparent power from the source to the n-th node or bus can be expressed as in Equation (7), and its supply current is the k-th iteration, shown in Equation (8), as follows:

$$S_{inj} = I_{inj} \cdot V_1 = \mathrm{S_{Load}} + \mathrm{S_{Loss}} = P_{Load} + jQ_{Load} + \left(\frac{P_{load} + Q_{load}}{V_2}\right)^2 Z \tag{6}$$

$$S_{inj-nth} = I_{inj-nth} \cdot V_{nth} = S_{Load-nth} + S_{Loss-nth} \tag{7}$$

$$I_i^k = I_i^r\left(V_i^k\right) + jI_i^i\left(V_i^k\right) = \left(\frac{P_i^k + jQ_i^k}{V_i^k}\right) \qquad i = 1 \ldots\ldots\ldots N \tag{8}$$

where S_{inj}, P_i, and jQi are the apparent, active, and reactive powers, respectively. The corresponding current and voltage injection at branches and buses are represented as I_i and

V_i. Pointing to Figure 2 again, the relationship between voltages at bus one and bus 2 is expressed as shown in Equations (8) and (9), as follows:

$$V_2 = V_1 - V_d \tag{9}$$

$$V_2 = V_1 - Z\left(\frac{P_{load} + Q_{load}}{V_2}\right)$$

Then, with several numbers (n) of buses, the n-th voltage at k iteration can be expressed in Equations (10) and (11) as follows:

$$V_i = V_{1i} - V_{di} = V_{1i} - Z\left(\frac{P_i^k + jQ_i^k}{V_i^k}\right) \tag{10}$$

But $Z = R_i + jX_i$

$$V_i^k = V_s - (R_i + jX_i)\left(\frac{P_i^k + jQ_i^k}{V_i^k}\right) \tag{11}$$

where Vs is the applied voltage and V_i^k is the n-th bus voltage after k iterations.

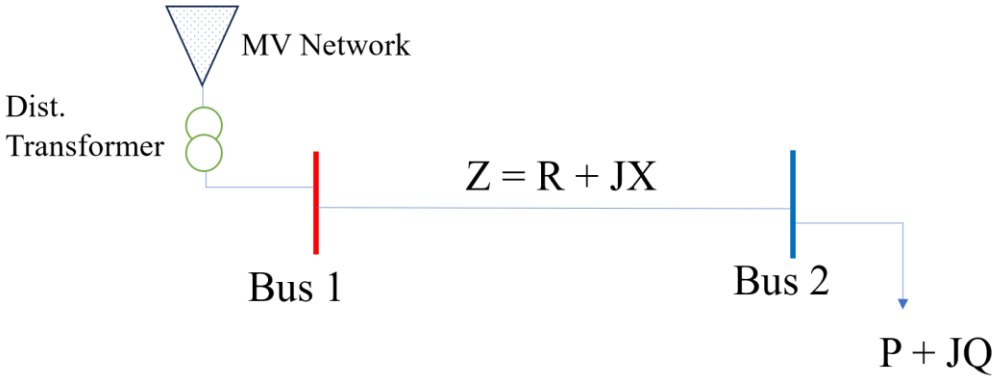


Figure 4. A simplified one-line diagram of an LV grid.

2.4. Load Flow

Load flow quantities are modelled in this study using the forward and backward (FB) method. Among the load flow methods, the FB has been noted for its good performance in distribution networks due to the high R/X ratio. In this method, branch currents are computed using the bus injection-to-branch voltage (BIBC) matrix. The nodal voltages are also computed using the branch current-to-bus voltage (BCBV) matrix. The BIBV is a lower triangular matrix with ones (1) entries in the upper diagonal and zeros (0) in the leading diagonal. The transposed of the BCBV matrix forms the BIBC matrix. The product of the resultant currents and voltages produce the system power flow matrices. The resultant power, voltage, and currents matrices can further be decomposed to their magnitudes and directions, since there are vector quantities. It is worth noting that the apparent power (S) solution matrix can be decomposed into active (P) and reactive power (Q) matrices, respectively.

The network losses (I^2R) and voltage drop (IZ) matrices can be also obtained. With the FB method, losses and voltage drops can be further decomposed into their constituents—thus resistive and reactive. Since there are several nodes and branches in LV networks, and power flow solutions are iterative with respect to buses and branches; the process starts at the reference bus through to the last bus of the network. Figure 4 shows a simplified one-line diagram of a low-voltage grid. The iteration process is outlined below:

1. Input parameters: the inputs parameters include number of nodes or buses; load (P + Q) buses: bus voltage limits (V_{min}, V_{max}): line impedances (R + jX); line section length (L_i); line capacity (amps); PV size (kWp); and RPS size ($kVAr$);
2. Base case: Firstly, compute I_n using the BIBC [a] and I_{load}, expressed in Equation (12). Calculate the bus voltages using the BCBV [b] matrices in Equation (13). The impedance matrix is formed by multiplying the BCBV matrix and the line impedance matrix (Z). In this context, I_n represents the current in the n-th branch, I_i is the n-th load current, and I_{npv} is the injection of the n-th PV system into the network;

$$[I_n] = [a][I_i - I_{npv} - I_{RPS}] \tag{12}$$

$$[V_n] = [V_s] - [Z_n][I_i - I_{npv} - I_{RPS}] \tag{13}$$

3. Calculate the following power flows as follows:
4. Apparent (S_{sec}), active, and reactive powers in the lines using Equation (14);
5. Lines losses ($Loss_{line}$) active and reactive losses are determined using Equation (15);
6. Apparent ($S_{injected}$), active, and reactive powers injections by using (16);

$$S_{\text{sec}} = \sum_{1}^{n} [I_n V_n] \tag{14}$$

$$Loss_{line} = \sum_{1}^{n} [I^2 Z] \tag{15}$$

$$S_{injected} = \sum_{1}^{n} [I_n V_n] + \sum_{1}^{n} [I^2 Z] \tag{16}$$

7. Iterate the process to determine the penetration for various PV injections;
8. Check whether the reactive power requirement is met with the PV injections. If yes, end the process; if no, execute step 4;
9. Repeat the process from 2 to include reactive power compensation (RSP)

2.5. Supercapacitor Model

Static capacitors (Cs) are used in this study to achieve RPS. The assumption is that internal resistance remains constant during charge and discharge cycles. The temperature effect on the electrolyte material and aging effect are not considered in this study. The charge redistribution in the capacitor remains constant for all voltage values and the capacitor current is assumed continuous, while its cell balancing is considered. The energy that the capacitor can store is given by Equation (17); based on the maximum power transfer theorem, the maximum power and maximum current of the capacitor (Cs) are given by Equation (18) and Equation (19), respectively, as follows:

$$E_{cs}(Wh) = \frac{1/2 \times CV_{cs}^2}{3600} \tag{17}$$

$$P_{cs}(W) = \frac{V_{cs}^2}{4 \times ESR} \tag{18}$$

$$\mathrm{I}_{cs}(A) = \frac{V_{cs}}{4 \times ESR} \tag{19}$$

where E_{cs} is the stored energy for 3600 s, C is the capacitance of the Super capacitor is in farad represented as C, V_{cs} is voltage of the bank, P_{cs} is the maximum power that the capacitor can deliver at any time, I_{cs} is the Cs bank maximum current, and the internal series resistance of the capacitor is ESR.

2.6. Case Study Analysis

A case study is presented in this section using the Obaa-Yaa substation in Drobo, Ghana. The analysis from the case study provides a real-world application of the technical and economic analysis of converting a low-voltage distribution grid into a solar PV microgrid.

2.6.1. Solar PV Electricity for Grid-to-Microgrid Conversion

The Obaa-Yaa substation located in Drobo has latitude of −2.81432 and longitude of 7.65622. A map of the study area is shown in Figure 5. The area highlighted with red line delineates the catchment zone for the substation, while the smaller red boxes identify the seven residences equipped with rooftop photovoltaic systems. There are abundance solar resources in the area with average daily radiation between 4.36 and 5.04 kWh/m^2. The average temperature and wind speed are 26.5 °C and 2.9 m/s, respectively [41]. Figure 1 shows Ghana's solar map to confirm, while Figure 6 depicts Drobo's yearly weather data obtained from RETScreen 4.0 software.

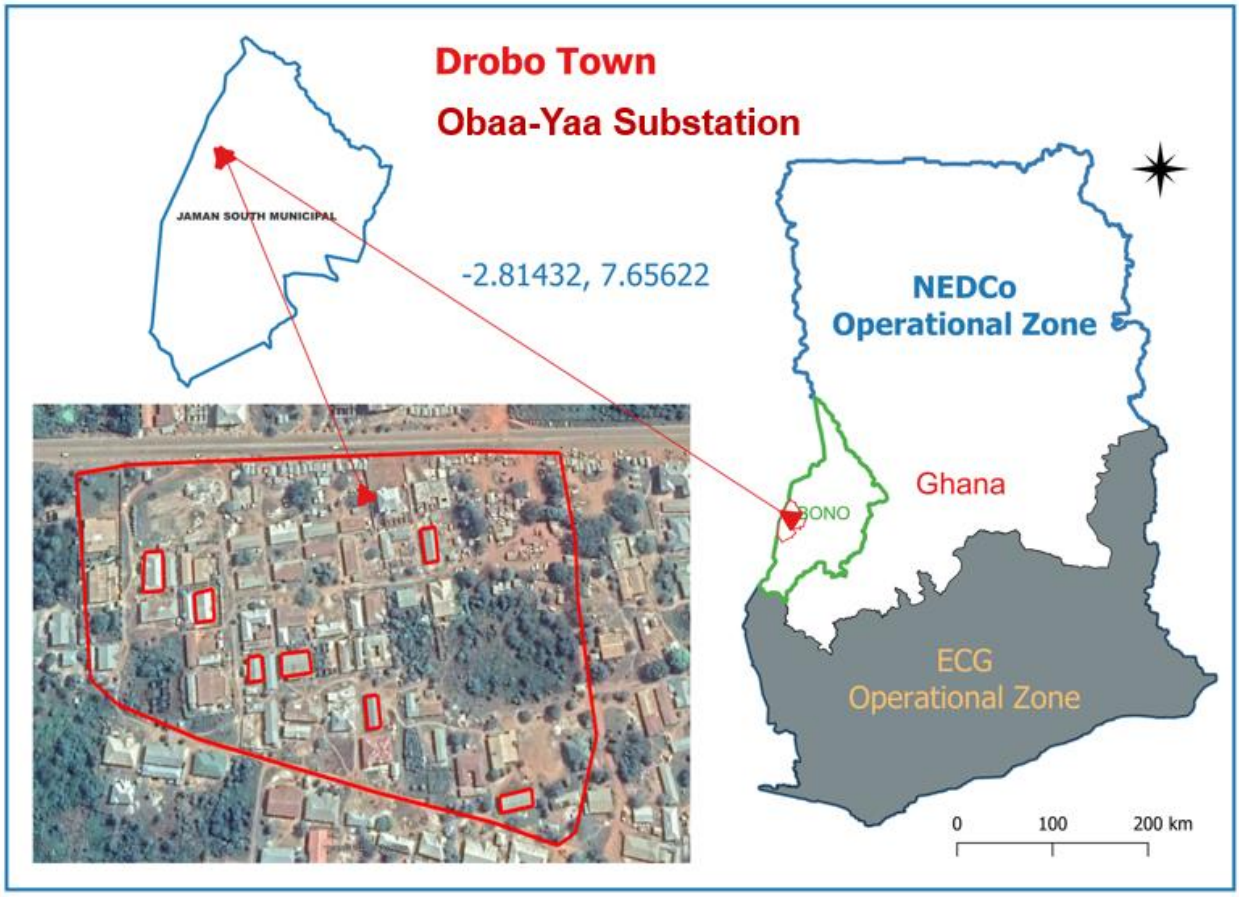


Figure 5. Study area map indicating structures selected for the microgrid conversion in red.

The conversion of the existing LV grid into a LV microgrid starts with the assessment of solar photovoltaic (PV) electricity potential in the area under consideration. Several factors are considered in this regard. These include the available annual solar radiation, the land area required and its cost to produce the desired energy to meet the demand, the construction of new lines for the PV plant grid integration, and the option of using a rooftop system.

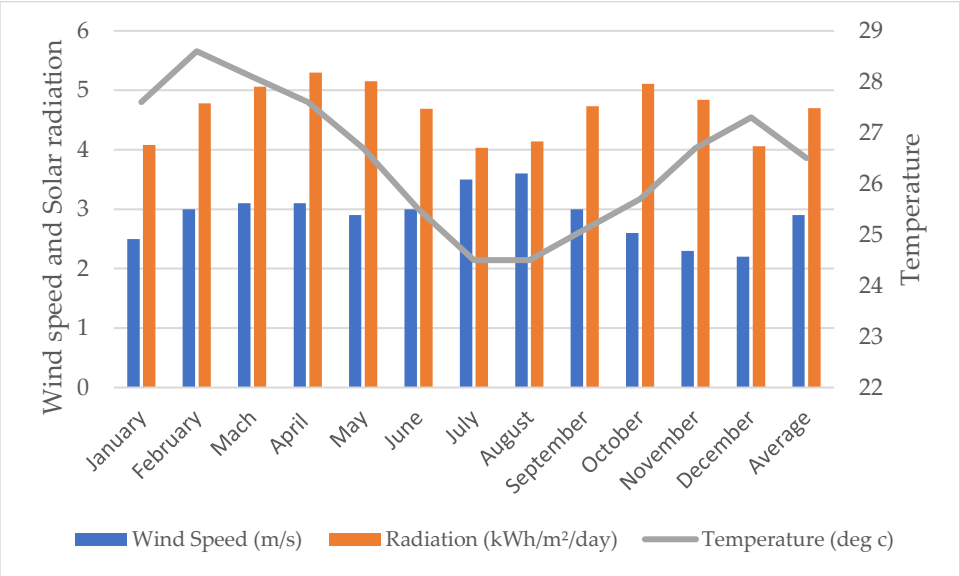


Figure 6. Drobo's yearly weather data.

2.6.2. Data Collection—Network and Consumer Data

On-site visits allow assessing the existing LV infrastructure to host the PV plants, distribution network layout, and potential constraints or limitations. Primary data were collected by measurement at the Obaa-Yaa substation. A clamp-on ammeter measured the consumers' service line currents. The measured parameters are (i) consumer load current and (ii) terminal voltage. This is called consumer load monitoring. The measurements were taken during the peak hours of the area (between 6 and 10 pm). The parameters of the clam-on ammeter used are HT 9021; IEC/EN 61010–1; CAT IV; 1000 A; and 1000 V [42]. The HT 9021 clamp meter is a product of ICS Schneider Messtechnik GmbH, Hohen Neuendorf, Germany. Secondary data, such as utility records and energy reports, were collected to supplement the primary data and provide additional context and background information. The consumers' energy consumption profiles on the substation were collected from the NEDCo Drobo Service Centre for further analysis. These data span one year. Understanding the consumer's load profile is expedient so that the capacity to meet the demand would not be compromised. These energy profiles are lumped, meaning they do not provide information on maximum demand and, hence, the field measurement. There are a total of 283 customers on the substation. Out of the total, residential constitutes 80%, while commercial is 20%. There are no special load tariff (SLT) customers in the area. In terms of energy consumption, 489,150 kWh was recorded by the Northern Electricity Distribution Company (NEDCo) in March 2022.

2.6.3. Solar PV System Sizing

Based on the collected data, a detailed technical assessment is conducted. The assessment involves analysing the study area's energy consumption profiles, load patterns, and solar resource availability. It also considers integrating solar PV systems with the existing distribution network, including system capacity, voltage regulation, and grid stability. Load management strategies are developed to optimise solar energy utilisation and balance supply and demand.

The average solar radiation in the area is 4.81 kilowatt-hours per square meter per day. Drobo has a vast land area that could be used for PV electricity generation. However, most of it is agricultural land, and using it for electricity generation can threaten food security—consequently, the choice of rooftop solar PV systems. Again, connecting a solar

plant to the grid from a distant location involves additional infrastructure costs, which would raise the project's overall expenses. Therefore, this study uses rooftop structures near the LV grid to be converted to a microgrid.

Let S_{eff} be the effective surface area of a rooftop of a given structure, and $S_{eff\ per\ stru}$ be the area per structure where solar PV is to be installed. Equation (20) describes the relationship between the two areas. The surface area ($S_{eff\ per\ stru}$) of the residential structures in the study area were estimated using the Google Earth Pro software 7.3.6.10201. Solar PV capacity (kW) is proportional to the cumulative surface area. Let the potential capacity of the PV plant be P_{total}. Then, the relationship between the capacity and the area for PV panel installation is shown in Equation (21). Equation (22) shows the number of panels needed for meeting the demand. After estimating each structure's surface area, the results were divided by 20 square feet (the maximum area of a 400 Wp solar module). The potential solar electricity harvested from the structures is estimated using Equation (23).

$$S_{eff} = \sum_{1}^{N} S_{eff\ \ per\ stru} \tag{20}$$

$$P_{total} = \frac{P_{panel}}{10^3}\acute{\eta}\cdot\left(\frac{S_{eff}}{P_{area}}\right) in\ kW \tag{21}$$

$$n = \frac{S_{eff}}{P_{area}} \tag{22}$$

$$E_{annual\ yeild} = \frac{365}{10^3}\acute{\eta}\cdot P_{panel}\cdot t\left(\frac{S_{eff}}{P_{area}}\right) \text{in kWh} \tag{23}$$

where $S_{eff\ per\ stru}$ is the total effective area of structures, P_{area} is the solar panel surface area, n is the number of panels required, P_{panel} is the output power of a single panel, t is the daily average sunshine hours, the system efficiency is $\acute{\eta}$, and $E_{annual\ yeild}$ is the yearly energy (kWh) yield.

2.7. Python Simulation

The existing LV grid is modelled in Python for simulations. The code development involves the definition of libraries and input parameters (loads, line characteristics, transformers, source bus voltage, PV injections, and reactive compensators). The BCBV and BIBC matrices were executed in load flow equations in the code. Lastly, graphs and tables showing load flow solutions were generated. The simulations evaluate hosting capacity PV injections on the LV network (415 or 240 V). The hosting capacity analysis emphases bus voltage, line losses, and loading on the transformer. The main input parameters used in the simulations are rating of transformer (kVA), and the transformer second bus voltage (V) and its no-load loss (2%) of the rating. Line impedance of 0.0579 + j0.0249 Ω/50 m was considered. Various consumers (capacity and location) as connected on the grid and the PV and RPS capacities placed on the network are shown in Appendix A, while Figure 7 shows the existing LV network diagram. The simulations scenarios performed are as follows:

1. Base case: simulating the actual state of the LV network with PV and RSP injections;
2. Scenario 1: simulation with the base case information and PV injections;
3. Scenario 2: simulation with the base case information, PV, and RSP (natural) injection;
4. Scenario 3: simulation with base case information, PV, and RSP (optimised) injection.

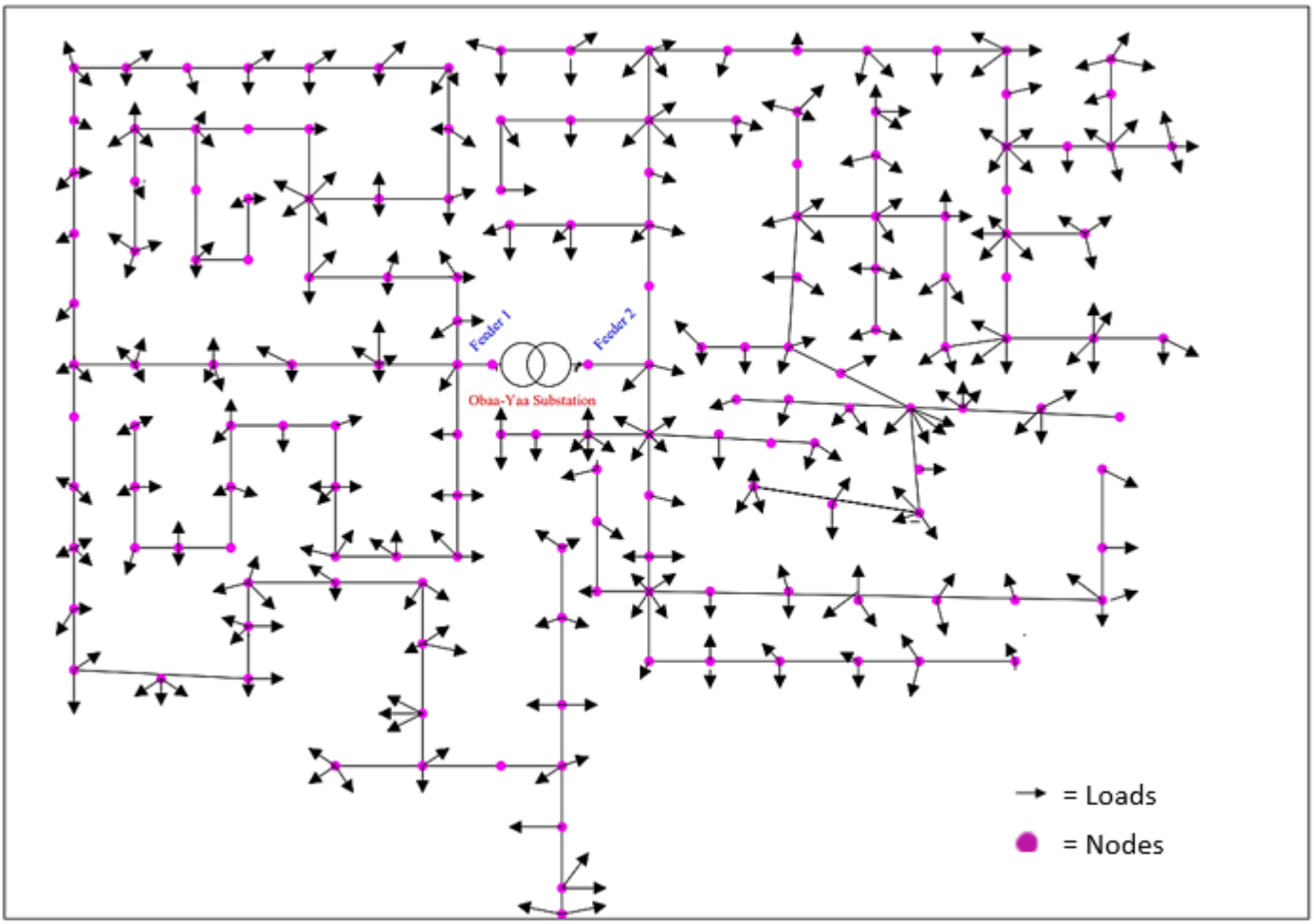


Figure 7. Study area (Obaa-Yaa substation) network topology.

2.8. Economic Analysis

2.8.1. Cost Analysis

The economic analysis in this work assesses the financial feasibility and cost implications of converting the low-voltage distribution network at the Obaa-Yaa substation into a solar-powered microgrid. The cost analysis considers the initial investment and operational and maintenance costs. The initial investment costs include procuring and installing solar PV panels, inverters, energy storage systems, and accessories required for installation and grid integration, which are necessary infrastructure upgrades. The upgrade costs of interconnection with the existing distribution network, such as transformers and distribution lines, are considered. Additionally, permitting, engineering, and project management costs are excluded from the analysis. The operational costs encompass maintenance and monitoring expenses, system management, and any necessary repairs or replacements over the system's lifetime. The storage system maintenance costs and battery replacements are factored into the analysis. If $RE_{subsidy}$ is the subsidy provided to encourage RE in Ghana, PV_{size} is capacity of the PV system in kWp. Then, the PV system's total capital expenditure (CAPEX) required for the microgrid conversion is calculated using Equations (24) and (25). At the same time, operational expenditure (OPEX) is estimated with Equation (26). The yearly OPEX is 1% of the capital expenditure. The 1% OPEX assumption is obtained in [33], since rooftop PV has minimal maintenance costs. The lithium-ion battery storage and inverter have lifespans between 10 and 15 years [27,33], and this was considered in the economic analysis. The inverter costs (GHS 3470/kW) reflect 2024 market quotes from

Accra-based suppliers. The annual OPEX will differ in the tenth and twentieth years due to the inverter and storage require replacement.

$$C_{gross} = P_{cost} + Inv_{cost} + BS_{cost} + Ass_{cost} + Cap_{cost} + Inst_{cost} + Other_{cost} \quad (24)$$

$$CAPEX = PV_{size} \times (P_{cost} + Inv_{cost} + BS_{cost} + Ass_{cost} + Cap_{cost} + Inst_{cost} + Othe_{cost}) - RE_{subsidy} \quad (25)$$

$$OPEX = \begin{cases} 1\% CAPEX \; from \; the \; 1st \; year \; to \; 25th \; year, \; excluding \; 10th \; and \; 20th \\ + \\ Inv_{cost} + BS_{cost} \; for \; the \; 10th \; year \; and \; 20th \; year \end{cases} \quad (26)$$

where C_{gross} is the PV plant cost (GHS/Wp), P_{cost} is the solar modules cost, Inv_{cost} is the grid-tie inverter cost, BS_{cost} is the cost of lithium battery storage, Ass_{cost} is the amalgamated accessories cost, and $Inst_{cost}$ is the installation cost.

2.8.2. Revenue Generation

The revenue generation potential of the solar-powered microgrid is assessed to determine the financial benefits and return on investment. The solar-powered microgrid is used to supply electricity directly to consumers within the Obaa-Yaa substation in Drobo. Firstly, the energy terms must be converted to monetary values. Suppose R_{mg} is the revenue due to energy (kWh) sold to the consumers within the microgrid. In that case, E_{mg} is the total electricity the PV plant generates in a year, and C is the charge per unit (kWh). Then, the expected R_{mg} sold in the project lifetime (25 years) from the PV plant is calculated using Equation (27). The degradation effect $(1 - D)^n$ of the PV plant is factored in since it influences PV's annual energy production.

$$R_{mg} = \sum_{1}^{25} \left(E_{mg,1} \times (1 - D)^n \right) \times C \quad (27)$$

2.9. Economic Evaluation

A financial evaluation of the solar-powered microgrid conversion is conducted to assess the viability of the proposed project. The net present value (NPV), profitability index (PI), internal rate of return (IRR), and payback period are the main financial indices used in this work. Equations (28) and (29) were used for the *NPV* and *IRR* analyses, whereas (30) and (31) were used to the IP, and DPP computations, respectively, as follows:

$$NPV = \sum_{n=1}^{N} \frac{Cash\,flow_n}{(1 + r)^n} - CAPEX \quad (28)$$

$$0 = \sum_{n=1}^{N} \frac{Cash\,flow_n}{(1 + IRR)^n} - CAPEX \quad (29)$$

$$PI = \frac{\sum CF_{inflows}}{\sum CF_{outflows}} \quad (30)$$

$$DPP = \frac{N_{rec} + \sum CF_{inflows}}{\sum CF_{outflows}} \quad (31)$$

where the discount rate is represented as r, N is the project life in years, $CF_{inflows}$ is the cash inflow, $CF_{inflows}$ is the discounted cash, and N_{rec} is the year before DPP occurs.

3. Results and Discussion

This section presents and discusses this study's findings. It first presents the technical results—load flow (voltage profile, power flows, and losses); then, the consumers'

demand analysis and solar energy production are followed. Lastly, the economics of the LV microgrid conversion are presented.

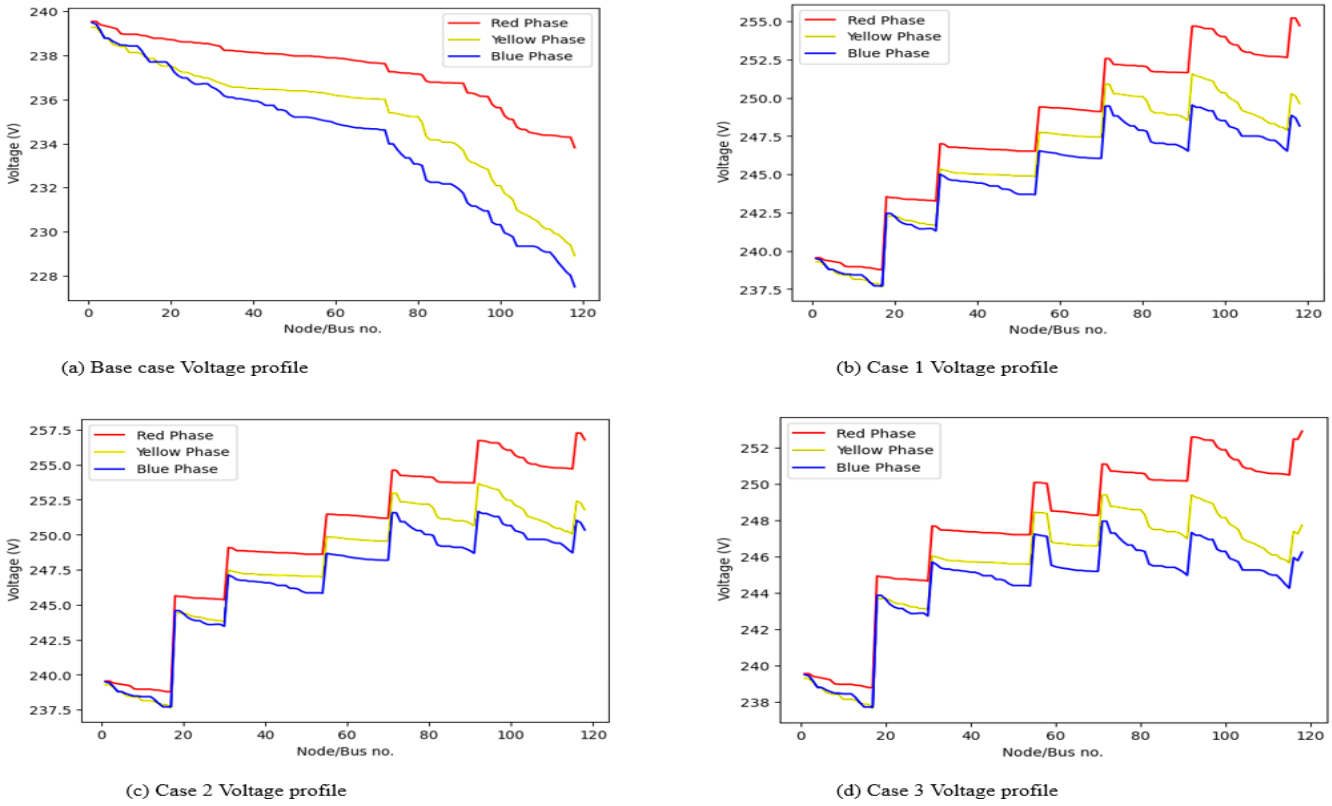
3.1. Load Flow Results

The section presents the results obtained from the load flow simulations as per scenarios stated in Section 3.6 (Python simulation).

3.1.1. Voltage Profile

Firstly, as the forward and backward method suggests, the branch currents were produced from the simulation's backward sweep. The highest currents were recorded at the end of the R, Y, and B substations, with the following recordings: 128.631 A, 240.97 A, and 273.36 A, respectively. Secondly, the bus voltages and line voltage drops were produced in the forward sweep. Thirdly, Power flows and losses were computed for all the scenarios. Voltage profiles from the simulations are shown in Figure 7.

In Figure 8a, the base case profiles for phases 1 (red), 2 (yellow), and 3 (blue) are shown. The supply voltage declined from 240 V to nearly 228 V due to the drops on the network resulting from the load currents and line section impedances. The minimum phase-wise voltages of R, Y, and B are 235 V, 229 V, and 228 V, respectively. Figure 8b–d shows the profiles (voltage) for cases 1, 2, and 3, orderly. The profile of case 1 increased at most nodes compared to the nominal voltage of 240 V. Under this scenario, the maximum and minimum voltages (see Figure 8b) were 255 V and 237.5 V, respectively. Figure 8c shows the voltage profile for case 2—the profile for this scenario is like case 1, just that the maximum voltage was slightly increased (257.5 V) compared to the 255 V in case 1. Figure 8d shows the profile for case 3—in this case, the maximum voltage (252 V) was slightly lower than that of cases 1 and 2 but higher than the base case (240 V). And there was no significant difference in the minimum voltage from cases 1 and 2.



(a) Base case Voltage profile

(b) Case 1 Voltage profile

(c) Case 2 Voltage profile

(d) Case 3 Voltage profile

Figure 8. Voltage profile.

3.1.2. Power Flows

The power flow results from the four scenarios are presented in Table 2. The apparent power recorded for the base case is 154.05 kVA, while its active and reactive demands were 144.11 kW and 54.45 kVAr, respectively. Case 1's apparent, active, and reactive demands were 128 kVA, −115.89 kW, and 54.45 kVAr, respectively. In case 2, 162.8 kVA, −115.8 kW, and 114.45 kVAr were recorded for the apparent, active, and reactive power demands, respectively. The apparent power, active power, and reactive power demands for case 3 are 115.8 kVA, −115.89 kW, and −0.55 kVAr, respectively.

Table 2. Load flow results.

Cases	Apparent Power (kVA)	Active Power (kW)	Reactive Power (kVAr)	Total Loss (kW)	Active Loss (kW)	Reactive Loss (kVAr)	Power Factor	Trafo Loading %	Phase Current (A)		
									R	Y	B
Base	154.05	144.11	54.45	10.98	4.67	9.93	0.935	75.4	128.63	240.97	273.36
Case 1	128	−115.89	54.45	6.01	5.65	−2.07	−0.9	62.7	245.51	160.9	143.4
Case 2	162.8	−115.8	114.45	9.24	4.25	−8.21	−0.711	79.81	273.4	217	208.97
Case 3	115.8	−115.89	−0.55	5.48	4.8	2.64	−0.99	56.7	243.3	136.6	107.8

It is worth noting that the external grid served the demand in the base case, and the solar PV system served the demand in cases 1, 2, and 3. After serving the demand, an excess of 115.8 kW was exported to the MV grid, representing a negative value.

In case 1, the system lacked a reactive of 54.45 kVAr since the grid was switched off and the supply to the network was entirely from the PV plants. This reactive demand necessitated the second case 2 and 3. In case 2, the reactive demand on the network rose to 114.45 kVAr due to the RPS configuration, which led to case 3. The new configuration (case 3) served the load's reactive demand, and nearly negligible (−0.55 kVAr) excess reactive power floated on the network.

3.1.3. Losses

After obtaining the network current in the backward sweep, the next step was to use the currents to calculate the power loss. In the power systems, power loss cannot be avoided but can be minimised with suitable engineering designs. Power loss assessment (magnitude and location) is the first step towards mitigation. Magnitudes and locations of power loss were assessed in all the scenarios.

The total loss recorded for the base case was 10.98 kW, with active and reactive components of 4.67 kW and 9.93 kW, respectively. Case 1's total loss was 6.01 kW (the active and reactive components were 5.65 kW and −2.07 kW, singly). In case 2, the total loss recorded was 9.24 kW, the active was 4.25 kW, and the reactive was −8.21 kW. In the last scenario (case 3), the total loss stood at 5.48 kW (active, 4.8 kW, and reactive, 2.64 kW). Figure 9a–d shows the system loss profiles for the base case, case 1, case 2, and case 3, respectively.

The phase-wise components of the loss profiles obtained from the base case scenario are shown in Figure 10. Figure 10a shows the total phase-wise components concerning R, Y, and B. Figure 10b–d show the vector components of the total (Figure 10a) for the R, Y, and B phases. The phase-wise components of the loss profiles for case 1 are shown in Figure 11. Figure 10 shows the total phase-wise components for R, Y, and B. The vector components of the total (Figure 11a) are shown in Figure 11a–c for the R, Y, and B phases, respectively. Figure 12 shows the total loss for case 2, while Figure 12a–c show the phase-wise vector components of Figure 12a as R, Y, and B, orderly. In Figure 13, the phase-wise components of the loss profiles for case 3 are shown. Figure 13a shows the total phase-wise components

concerning R, Y, and B. Figure 13a–c show the vector components of the total (Figure 11a) for the R, Y, and B phases.

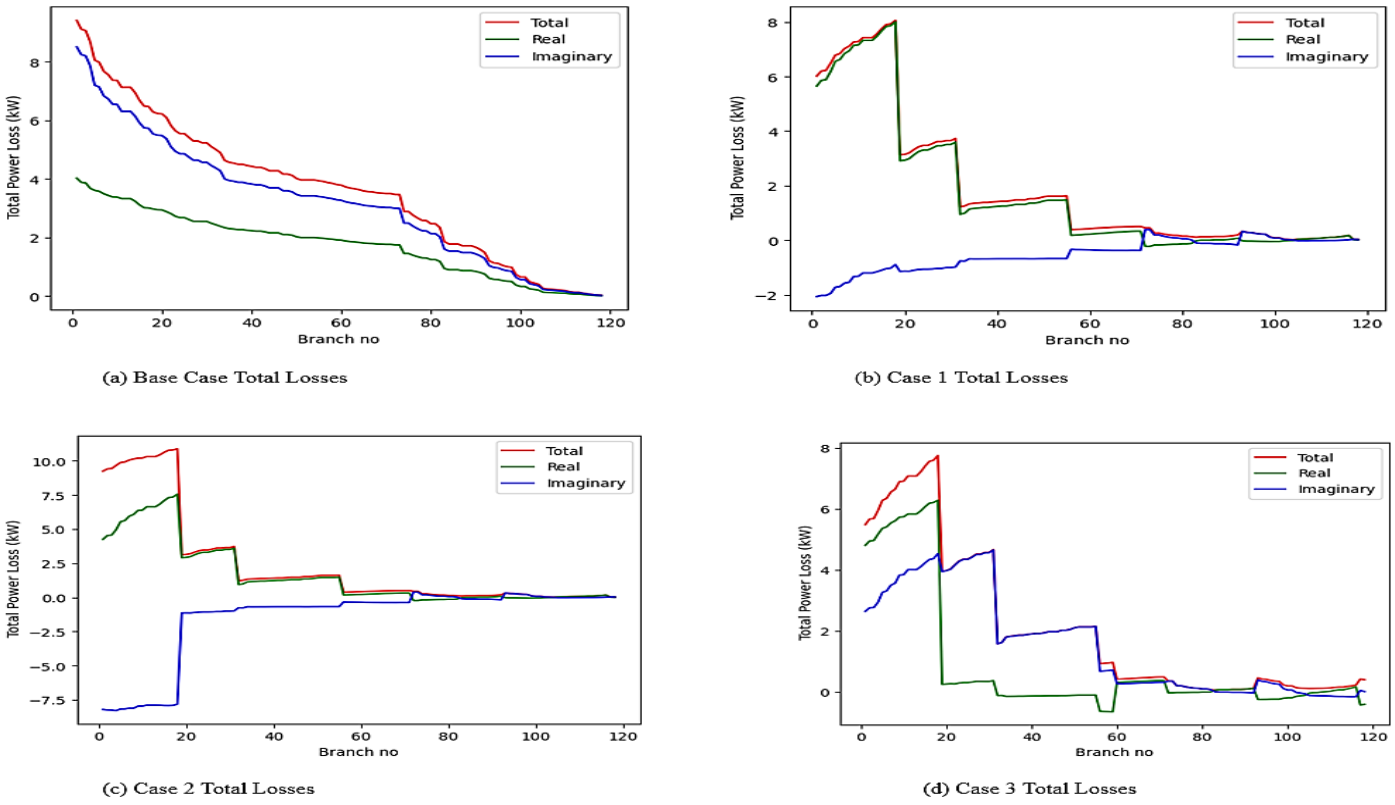


Figure 9. Scenarios of loss profiles.

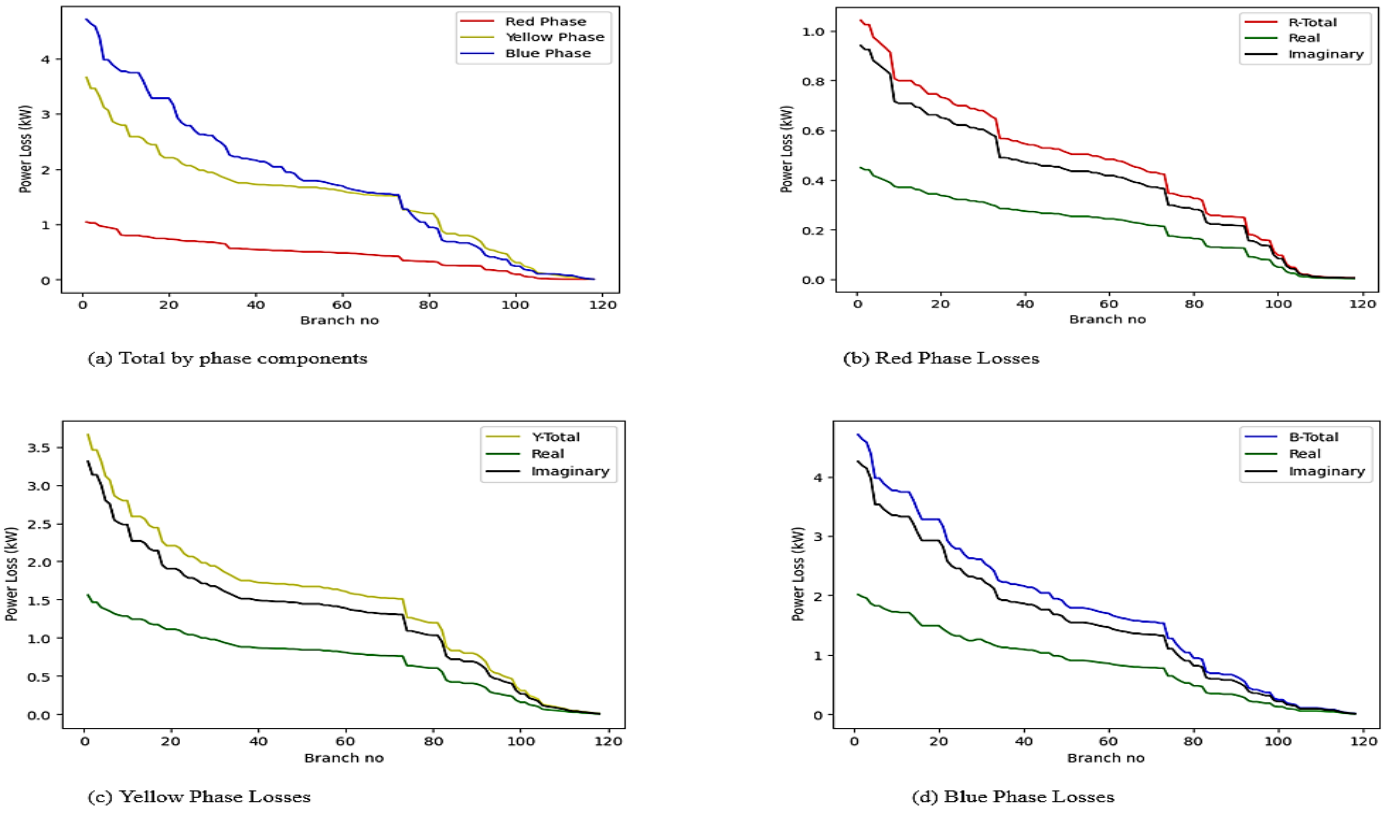
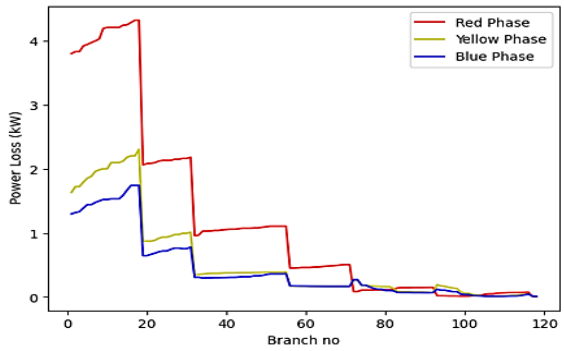
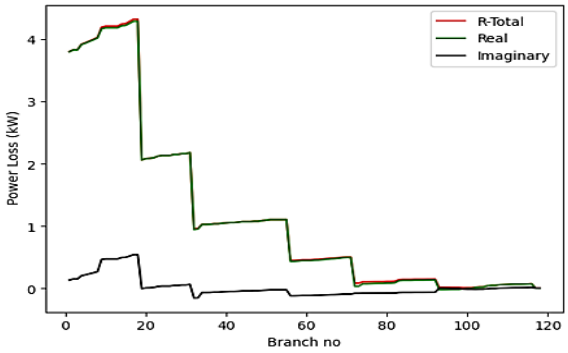


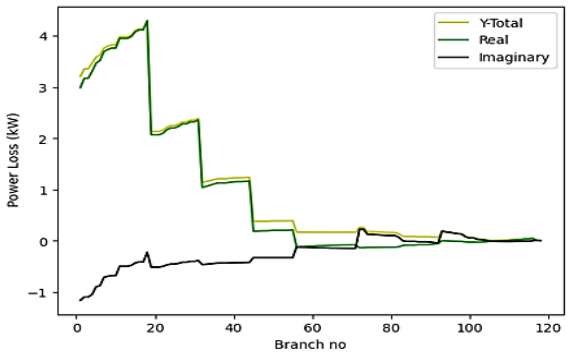
Figure 10. Base case loss profile.



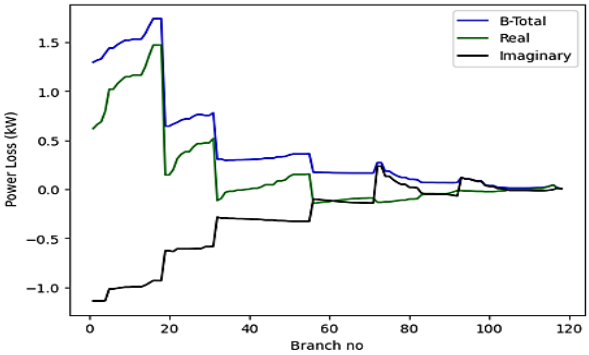
(a) Total by phase components



(b) Red Phase Losses

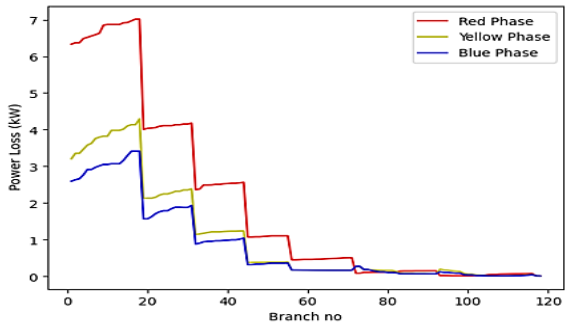


(c) Yellow Phase Losses

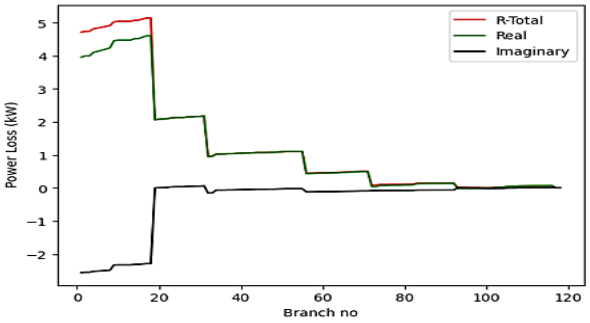


(d) Blue Phase Losses

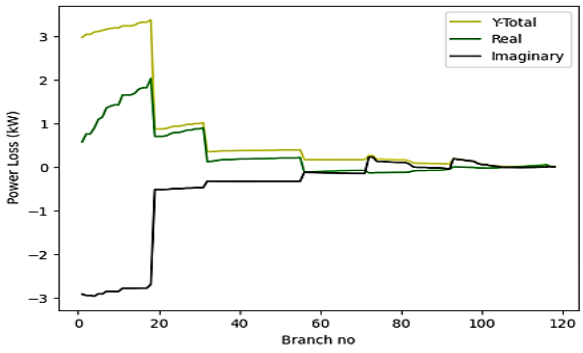
Figure 11. Case 1 loss profile.



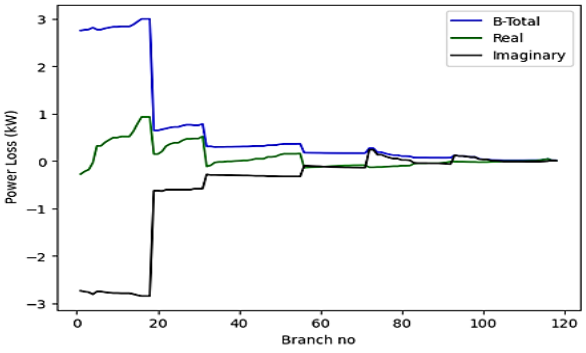
(a) Total by Phase components



(b) Red Phase Losses



(c) Yellow Phase Losses



(d) Blue Phase Losses

Figure 12. Case 2 loss profile.

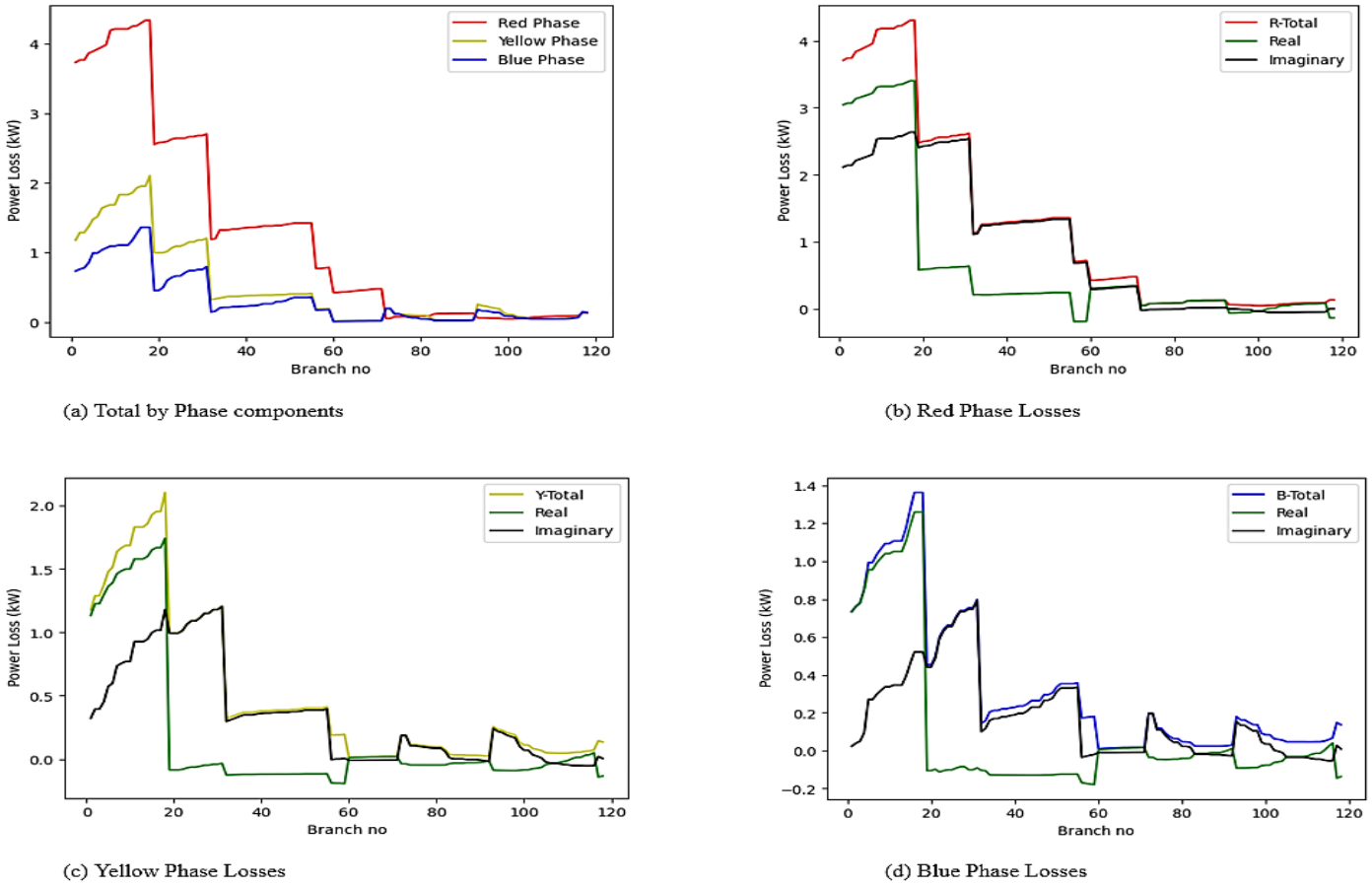


Figure 13. Case 3 loss profile.

3.2. Consumer Demand Analysis

There are several customers on the Obaa-Yaa substation. In 2022, these customers' total annual energy demand on the substation was 489,150 kWh. This energy in cedis terms amounted to GHS 388,286.04. The month-by-month consumer consumption and respective billed amounts are shown in Figure 14. The highest and lowest energy demand occurred in March 2022 and December 2022. This consumption is a true reflection of Drobo's energy demand. According to NEDCo, March has the hottest weather conditions, and December has the coldest weather conditions throughout the year. These accounted for the highest and lowest demand. The billed amount shown in Figure 14 includes service and statutory charges. Based on NEDCo's data, decoupling the service and statutory charges from the energy cost was nearly impossible. October 2022 saw the highest billed amount (GHS 41,714), though not the highest consuming month. This hike is attributed to the electricity tariff increase in September 2022.

3.3. PV Energy Production and Economics

Electricity production from solar PV plants at the Obaa-Yaa substation was done based on the consumer's energy requirements. It was expedient to assess the possibility of installing the PV modules on the rooftop of the residential consumer's structures in the study area. The area has several residential and commercial structures, but based on the consumer's demand for the Obaa-Yaaa substation, only seven (7) structures were selected for rooftop electricity production. The structure choice was based on the spatial distribution of structures and random selection along the LV network. A GIS web-based application (Google Earth Pro) was used for the seven randomly selected structures' surface areas assessment. A safety factor of 0.9 was applied to obtain the usable or effective area ($A_{eff.}$). It

is important to apply this safety factor since not all the measured areas of the structure can have PV panels installed.

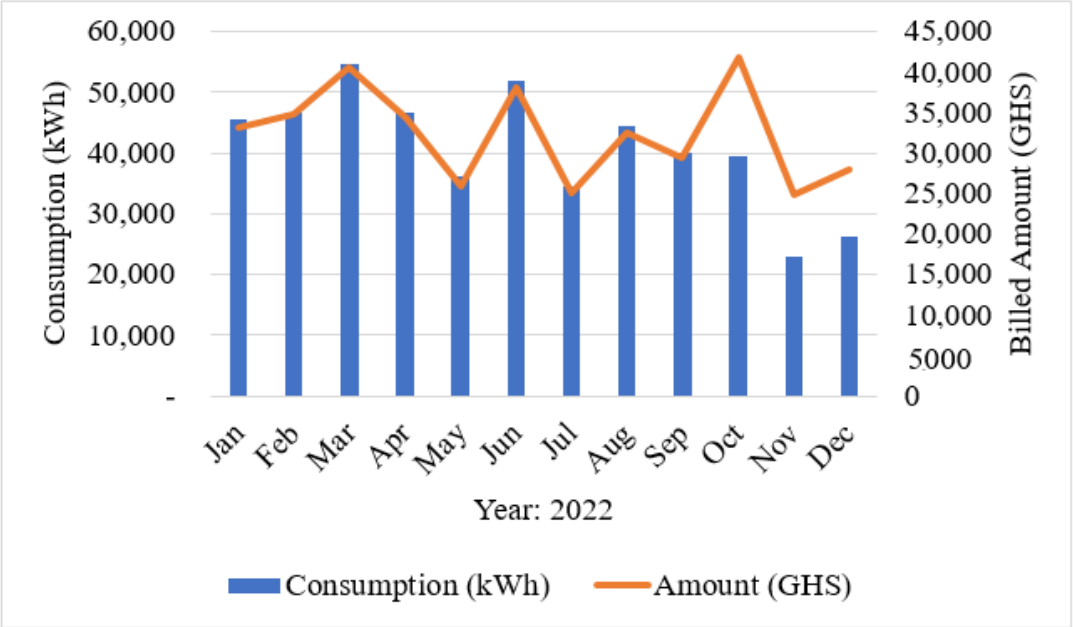


Figure 14. Obaa-Yaa substation consumers' energy demand profile.

Table 3 shows the results from the Google Earth estimation. The total surface area estimated from the seven structures is 17,167.50 square feet, and the corresponding number of solar panels the rooftop can accommodate is 858, based on Equation (21). A standard solar panel surface area is approximately 20 sq. Ft. From Equation (22), the generation capacity based on the 858 number of solar panels is 343 kWp, and the potential daily, monthly, and annual energy production (Equation (23)) is 1879.84 kWp, 56,395.24 kWh, and 676,742.85 kWh, respectively. The estimation assumed a system efficiency of 0.9. This study uses a maximum peak sun hours of 6 h at 5.04 kWh/m^2 per day. A variability factor was applied for safety since the sunshine varies from no to peak sunshine. This study considered variation in the sun's radiation in a range of 0 and 1. A 0 means no sunshine, and a 1 means maximum sunshine. Figures 15–17 show the prospective daily, monthly, and annual energy production profiles. The monthly profile is affected by the climatic changes in sunshine throughout the year, while the yearly energy profile is affected by the degradation factor of the solar panels.

Table 3. Energy production analysis.

No.	Name of Structure	Measured Area (ft^2)	Effective Area with a Safety Factor of 0.9 (ft^2)	No. of Panels per Structure	Power Production Capacity (kWp)	Energy/y (kWh)	Energy/mon (kWh)	Energy/d (kWh)
1	H1	4148	3733	187	75	147,162.74	12,263.56	408.79
2	H2	3255	2930	146	59	115,480.89	9623.41	320.78
3	H3	2619	2357	118	47	92,916.88	7743.07	258.10
4	H4	2883	2595	130	52	102,283.07	8523.59	284.12
5	H5	1993	1794	90	36	70,707.65	5892.30	196.41
6	H6	2410	2169	108	43	85,501.98	7125.17	237.51
7	H7	1767	1590	80	32	62,689.63	5224.14	174.14
	Total	19,075.00	17,167	858	343	676,742.85	56,395.24	1879.84

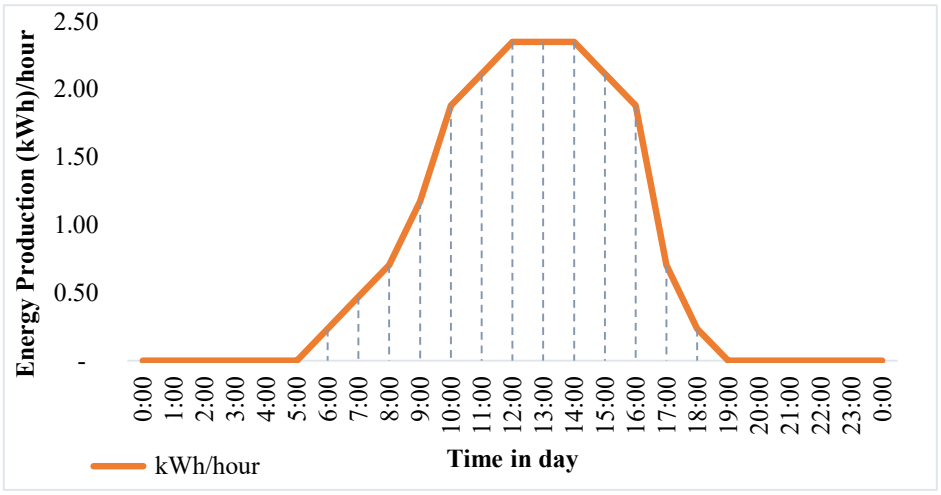


Figure 15. Daily generation profile.

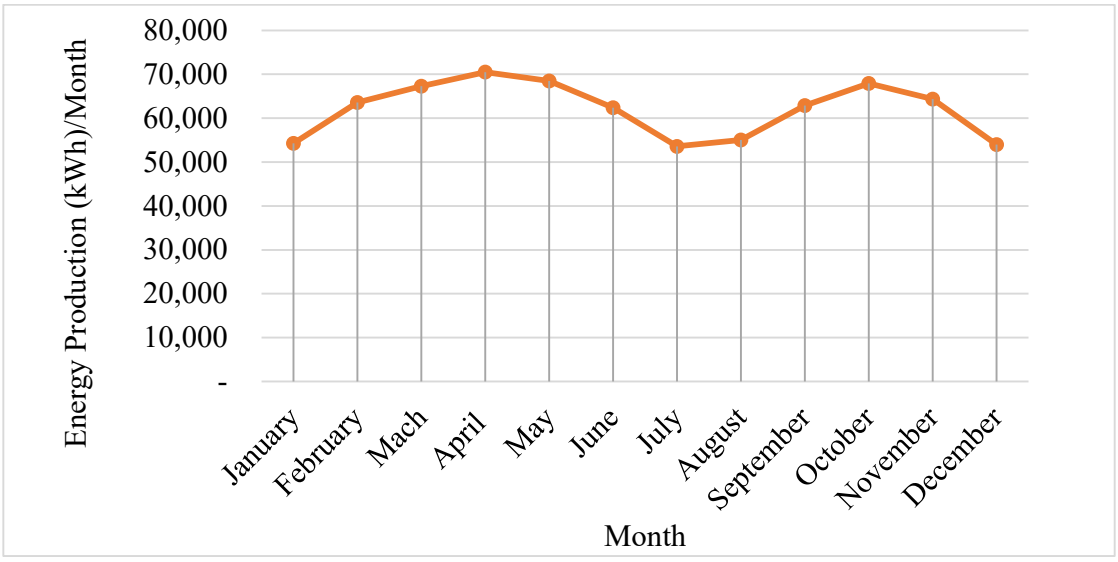


Figure 16. Monthly generation profile.

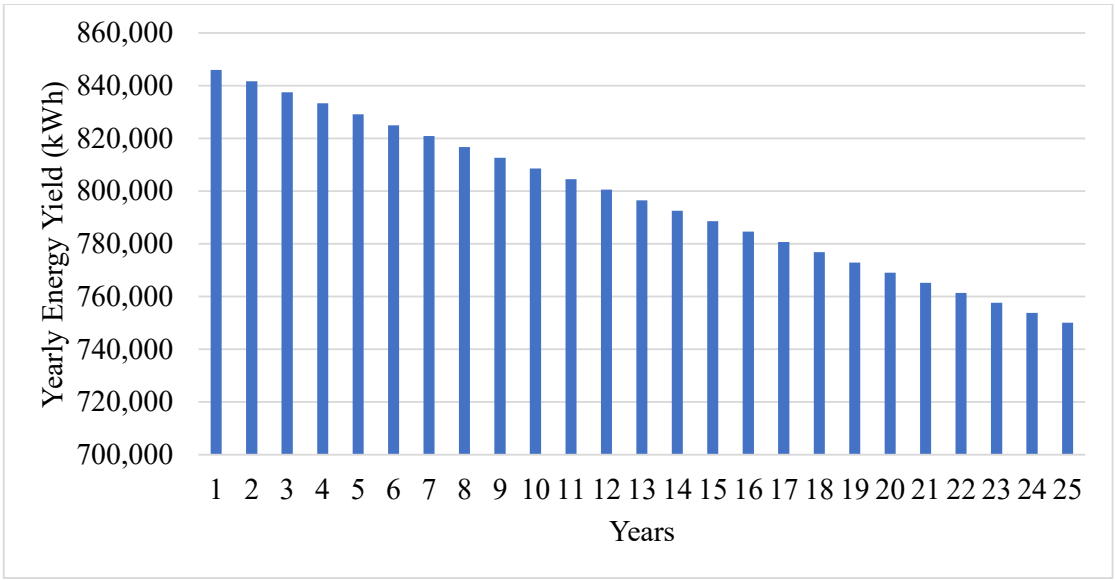


Figure 17. Yearly generation profile.

3.4. The Conventional LV Grid-to-Microgrid Conversion Economics

The section presents the economics of converting the LV grid to a microgrid. Investors are interested in this aspect. Since the objective function is about making the grid stand-alone with PV electricity, the system configuration is a PV system with storage and reactive support. To achieve higher economic returns in the future and to ensure optimal operation, the system was 80% oversized. The study uses Microsoft Excel in the Office 365 suite for the economic assessment. The projects' CAPEX is shown in Table 4. The CAPEX of the project was estimated at GHS 7,167,790, while the OPEX is GHS 71,677.9. The cost of the grid infrastructure is not considered in this study. Since the maintenance requirement of the solar PV project is minimal, its annual OPEX is always low. This study did not consider others microeconomic variables (such as inflation), but used a 10% discount rate. The battery bank and inverter strings were assumed to be replaced in the 10th and 20th years of their operations. The costs are due to the battery bank and inverters replacement presents additional capital injection in year 10 and 20. The cedi-to-the United States dollar exchange rate was GH11.37 to USD1. The economic results are shown in Table 5. An NPV of GHS 2,119,288.91 was obtained. Figure 18 shows the project's NPV curve in a 25-year period at 5 years intervals. The IRR, IP, and DPB are 17%, 1.2, and 10 years, respectively. These indices suggest that it is financially viable to convert existing conventional LV networks into PV microgrids.

Table 4. CAPEX.

Item	Rating	Unit of Measurement	Qty	Unit Cost (GHS)	Amount (GHS)
Panel	400	W	858	2700	2,317,613
Inverter	1	kW	430	3470	1,489,281
Battery	1	kWh	1175	1620	1,903,339
Capacitor	32	kVAr	1	30,000	30,000
Ass		lot	1	1,000,000	571,023
Installation		lot	1	2,080,208	285,512
Others		lot	1	3,846,956	571,023
Total					7,167,790

Table 5. Econometrics results.

Economic Indicator	Value
NPV	GHS 2,119,288.91
IRR	17%
DPP	10
Ip	1.2

3.5. Policy Implications

The outcomes of this study hold important policy relevance for electricity planners, government officials, and key stakeholders engaged in Ghana's ongoing energy transition, especially at the local and district levels. Integrating rooftop photovoltaic (PV) systems into existing low-voltage (LV) networks offers a practical and sustainable route to strengthening energy access, reliability, and environmental sustainability.

This research highlights the value of rooftop PV systems in enhancing and reinforcing the aging and often strained LV distribution networks, particularly in rural and peri-urban areas. Policymakers should formulate targeted strategies at both national and district levels to promote the hybridization of traditional grids with decentralized renewable energy solutions. Such grid modernization efforts can increase efficiency, lower transmission losses, and improve electricity service, especially in underserved communities.

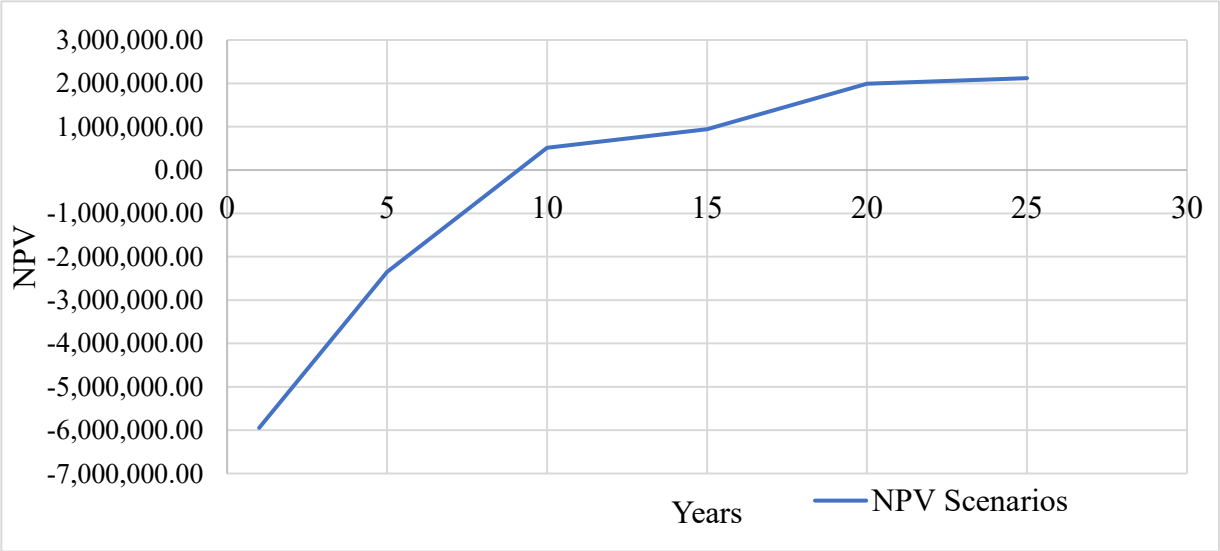


Figure 18. NPV over 25 years.

High upfront costs remain a major barrier to the widespread adoption of rooftop PV systems. To overcome this, the government and financial institutions should consider the following: Introducing subsidies, tax incentives, and exemptions for solar equipment. Providing access to low-interest loans or green finance options through dedicated energy funds and microfinance schemes. Fostering public–private partnerships (PPPs) to attract private investment in solar microgrid development. Such financial mechanisms are essential to lower investment risks and promote inclusive participation in the renewable energy sector.

The successful rollout of decentralized energy solutions hinges on coordinated engagement between all stakeholders. These include government bodies, local communities, and private sector partners, who deliver technological innovation, implementation capacity, and financing. Policies should prioritize participatory approaches, ensuring local stakeholders are actively involved and benefit from long-term project sustainability and ownership.

A shortage of skilled professionals poses a significant obstacle to rooftop PV deployment in many regions. Addressing this challenge requires a focus on the following: Establishing vocational training programs to develop local expertise in system installation, maintenance, and repair. Promoting research and innovation through partnerships with academic institutions and energy research centres. Conducting public education and outreach campaigns to increase awareness of solar energy's economic and environmental advantages. These capacity-building efforts should be integrated into broader national energy strategies and supported by international development organizations. By addressing these policy dimensions, Ghana can create a more resilient, inclusive, and sustainable electricity sector powered by distributed solar energy solutions.

3.6. Future Research and Recommendations

Conducting additional case studies in different geographical locations and with varying characteristics will provide a deeper understanding of the technical and economic implications of converting low-voltage distribution networks into solar-powered microgrids. This will help assess the generalizability of the findings and recommendations in different contexts.

While transient stability and short-circuit analysis are critical for dynamic grid behavior, this work prioritises steady-state techno-economic feasibility. Future studies will incorporate dynamic modelling.

4. Conclusions

In conclusion, this study has presented a comprehensive technical and economic analysis of converting a low-voltage distribution network into a solar-powered microgrid, through a case study (Obaa-Yaa substation in Drobo, Ghana). This research has explored the technical and economic feasibilities and implications of implementing solar-powered microgrid conversion. The grid stability assessment assessed the solar PV plant's hosting capacity (voltage and losses) on the grid. In contrast, the system performance evaluation evaluated the overall performance of the solar-powered microgrid. From an economic point of view, this study shows that the microgrid can generate revenue from energy sales to consumers on the grid to cover its cost. A net present value of GHS 2,119,288.00, internal rate of returns of 17%, profitability index of 1.2, and discounted payback period of 10 years were obtained from this study, signifying the economic viability of the proposed project. The findings of this research can serve as a foundation for further studies and guide the implementation of solar-powered microgrids in Ghana, contributing to the transition towards sustainable and decentralised electricity supply.

This study has two primary limitations:

a. The cost of replacing the existing LV grid infrastructure was not considered in this work and it could potentially reduce the financial prospect;
b. Ghana's rainy season (June–September) reduces PV output, which introduces very high intermittencies during the period, necessitating grid backup or hybrid systems.

Transient stability and short-circuit analysis are not considered.

Author Contributions: Conceptualization, F.K. and D.A.; methodology, F.K., D.A. and F.P.; software, F.P.; validation, F.K., D.A. and F.P.; formal analysis, F.K. and D.A.; data curation, F.K., D.A. and F.P.; writing—original draft preparation, F.K., D.A. and F.P.; writing—review and editing, F.K. and F.P.; supervision, Z.F., L.F.; funding acquisition, F.K., D.A. All authors have read and agreed to the published version of the manuscript.

Funding: This research received no external funding. However, Sunyani Technical University supported in the payment of the APC.

Data Availability Statement: The datasets used in this study can found in Appendix A. Details of the data (if required) could be provided upon request from the corresponding author.

Conflicts of Interest: The authors declare no conflicts of interest.

Appendix A. Load, PV Generation, and RSP Capacities

Node No.	Load kVA			Measured Load Terminal Voltage (V)			PV (kWp)	RPS (kVAr)	
	R	Y	B	R-N	Y-N	B-N		Natural	Optimised
1	0.27	1.61	0.55	241.9	243.6	239.6			
2	0.00	0.00	0.36	241.7	243.5	239.4			
3	0.77	1.19	1.39	241.6	243.2	239.2			
4	0.21	0.36	0.45	241.4	242.9	239.1			
5	0.24	0.46	0.00	241.2	242.6	238.9			
6	0.24	0.48	0.68	241.1	242.3	238.7			2.3
7	0.26	0.36	0.47	240.9	242.0	238.5			
8	0.43	0.24	0.43	240.7	241.7	238.3			
9	0.14	0.00	0.00	240.6	241.4	238.2			
10	0.00	0.63	0.21	240.4	241.1	238.0	93	2.3	
11	0.00	0.00	0.00	240.2	240.8	237.8			
12	0.00	0.00	0.00	240.0	240.5	237.6			

Node No.	Load kVA			Measured Load Terminal Voltage (V)			PV (kWp)	RPS (kVAr)	
	R	Y	B	R-N	Y-N	B-N		Natural	Optimised
13	0.29	0.31	1.04	239.9	240.2	237.4			
14	0.05	0.79	1.42	239.7	239.9	237.3			
15	0.29	0.29	1.23	239.5	239.6	237.1			
16	0.29	0.00	0.00	239.4	239.3	236.9			
17	0.00	0.53	0.00	239.2	239.0	236.7			2.9
18	0.00	0.55	0.00	239.0	238.7	236.5	73	2.9	
19	0.24	0.00	0.00	238.9	238.4	236.4			
20	0.05	0.00	1.02	238.7	238.1	236.2			
21	0.12	0.31	0.76	238.5	237.8	236.0			
22	0.31	0.76	0.83	238.3	237.5	235.8			
23	0.13	0.39	0.45	238.2	237.2	235.6			
24	0.00	0.00	0.00	238.0	236.9	235.5			
25	0.00	0.36	0.87	237.8	236.6	235.3			
26	0.21	0.52	0.59	237.7	236.3	235.1			
27	0.00	0.00	0.00	237.5	236.0	234.9			
28	0.14	0.42	1.12	237.3	235.7	234.7			
29	0.00	0.00	0.00	237.2	235.4	234.6			
30	0.21	0.36	0.78	237.0	235.1	234.4			
31	0.23	0.44	0.42	236.8	234.8	234.2	59	3.7	3.7
32	0.15	0.33	0.67	236.6	234.5	234.0			
33	0.28	0.33	0.29	236.5	234.2	233.8			
34	0.00	0.36	0.31	236.3	233.9	233.7			
35	0.03	0.31	0.00	236.1	233.6	233.5			
36	0.15	0.00	0.34	236.0	233.3	233.3			
37	0.00	0.00	0.00	235.8	233.0	233.1			
38	0.15	0.17	0.20	235.6	232.7	232.9			
39	0.08	0.13	0.10	235.5	232.4	232.8			
40	0.08	0.05	0.26	235.3	232.1	232.6			
41	0.00	0.00	0.00	235.1	231.8	232.4			
42	0.10	0.08	0.38	234.9	231.5	232.2			
43	0.15	0.06	0.61	234.8	231.2	232.0			
44	0.00	0.00	0.00	234.6	230.9	231.9	65	4.8	4.8
45	0.00	0.00	0.00	234.4	230.6	231.7			
46	0.08	0.13	1.03	234.3	230.3	231.5			
47	0.00	0.00	0.00	234.1	230.0	231.3			
48	0.18	0.08	0.30	233.9	229.7	231.1			
49	0.13	0.19	0.91	233.8	229.4	231.0			
50	0.14	0.00	0.51	233.6	229.1	230.8			
51	0.00	0.00	0.00	233.4	228.8	230.6			
52	0.00	0.00	0.00	233.2	228.5	230.4			
53	0.00	0.00	0.00	233.1	228.2	230.2			
54	0.00	0.22	0.13	232.9	227.9	230.1			
55	0.15	0.00	0.17	232.7	227.6	229.9	45	4	4
56	0.00	0.19	0.25	232.6	227.3	229.7			
57	0.12	0.00	0.22	232.4	227.0	229.5			
58	0.16	0.23	0.18	232.2	226.7	229.3			
59	0.00	0.13	0.12	232.1	226.4	229.2			
60	0.00	0.28	0.44	231.9	226.1	229.0			
61	0.15	0.13	0.24	231.7	225.8	228.8			
62	0.05	0.05	0.22	231.5	225.5	228.6			
63	0.15	0.15	0.13	231.4	225.2	228.4			
64	0.18	0.20	0.22	231.2	224.9	228.3			

Node No.	Load kVA			Measured Load Terminal Voltage (V)			PV (kWp)	RPS (kVAr)	
	R	Y	B	R-N	Y-N	B-N		Natural	Optimised
65	0.15	0.00	0.19	231.0	224.6	228.1			
66	0.07	0.10	0.00	230.9	224.3	227.9			
67	0.15	0.10	0.17	230.7	224.0	227.7			
68	0.21	0.00	0.03	230.5	223.7	227.5			
69	0.08	0.05	0.07	230.4	223.4	227.4			
70	0.00	0.00	0.00	230.2	223.1	227.2	54	4	4
71	0.13	0.10	0.22	230.0	222.8	227.0			
72	0.05	0.00	0.00	229.8	222.5	226.8			
73	1.88	3.16	3.28	229.7	222.2	226.6			
74	0.00	0.00	0.00	229.5	221.9	226.5			
75	0.14	0.24	1.34	229.3	221.6	226.3			
76	0.14	0.18	1.11	229.2	221.3	226.1			
77	0.05	0.25	0.86	229.0	221.0	225.9			
78	0.00	0.18	0.00	228.8	220.7	225.7			
79	0.20	0.05	1.43	228.7	220.4	225.6			
80	0.00	0.00	0.00	228.5	220.1	225.4			
81	0.21	1.36	0.35	228.3	219.8	225.2			
82	1.44	3.34	3.49	228.1	219.5	225.0			
83	0.25	0.75	0.49	228.0	219.2	224.8			
84	0.00	0.00	0.00	227.8	218.9	224.7			
85	0.00	0.00	0.00	227.6	218.6	224.5			
86	0.14	0.57	0.40	227.5	218.3	224.3			
87	0.00	0.00	0.00	227.3	218.0	224.1			
88	0.00	0.00	0.00	227.1	217.7	223.9			
89	0.05	0.31	0.58	227.0	217.4	223.8			
90	0.02	0.69	0.70	226.8	217.1	223.6			
91	0.05	0.95	0.96	226.6	216.8	223.4			
92	2.22	2.10	2.28	226.4	216.5	223.2		4	4
93	0.05	0.69	0.76	226.3	216.2	223.0			
94	0.25	0.26	0.00	226.1	215.9	222.9			
95	0.47	0.63	0.62	225.9	215.6	222.7			
96	0.05	0.41	0.53	225.8	215.3	222.5			
97	0.07	0.39	0.00	225.6	215.0	222.3			
98	1.80	2.49	2.71	225.4	214.7	222.1			
99	0.74	1.33	0.55	225.3	214.4	222.0			
100	0.00	0.00	0.00	225.1	214.1	221.8			
101	1.91	1.84	1.97	224.9	213.8	221.6			
102	0.74	0.60	0.41	224.7	213.5	221.4			
103	0.10	0.87	0.53	224.6	213.2	221.2			
104	1.80	2.52	2.26	224.4	212.9	221.1			
105	0.54	0.55	0.00	224.2	212.6	220.9			
106	0.00	0.45	0.00	224.1	212.3	220.7			
107	0.69	0.47	0.00	223.9	212.0	220.5			
108	0.18	0.66	0.00	223.7	211.7	220.3			
109	0.18	0.51	0.26	223.6	211.4	220.2			
110	0.25	1.14	0.75	223.4	211.1	220.0			
111	0.09	0.72	0.40	223.2	210.8	219.8			
112	0.00	0.00	0.00	223.0	210.5	219.6			
113	0.07	1.01	1.12	222.9	210.2	219.4			
114	0.11	0.25	1.36	222.7	209.9	219.3			
115	0.20	0.92	1.14	222.5	209.6	219.1			

Node No.	Load kVA			Measured Load Terminal Voltage (V)			PV (kWp)	RPS (kVAr)	
	R	Y	B	R-N	Y-N	B-N		Natural	Optimised
116	0.04	0.96	1.18	222.4	209.3	218.9	40	5.4	5.4
117	0.04	0.71	0.83	222.2	209.0	218.7			
118	2.46	2.55	2.73	222.0	208.7	218.5			
Total	28.29	52.58	61.38				429.19	31.10	31.10

References

1. Peprah, F.; Gyamfi, S.; Amo-boateng, M.; Effah-donyina, E. Impact assessment of grid tied rooftop PV systems on LV distribution network. *Sci. Afr.* **2022**, *16*, e01172. [CrossRef]
2. Asante, K.; Gyamfi, S.; Amo-Boateng, M. Techno-economic analysis of waste-to-energy with solar hybrid: A case study from Kumasi, Ghana. *Sol. Compass* **2023**, *6*, 100041. [CrossRef]
3. Peprah, F.; Gyamfi, S.; Effah-donyina, E.; Amo-boateng, M. e-Prime-Advances in Electrical Engineering, Electronics and Energy Evaluation of reactive power support in solar PV prosumer grid. *e-Prime-Adv. Electr. Eng. Electron. Energy* **2022**, *2*, 100057. [CrossRef]
4. Poongothai, S.; Srinath, S. Power quality enhancement in solar power with grid connected system using UPQC. *Microprocess Microsyst.* **2020**, *79*, 103300. [CrossRef]
5. Sechilariu, M.; Locment, F. *Urban DC Microgrid: Intelligent Control and Power Flow Optimization*, 1st ed.; Elsevier: Amsterdam, The Netherland, 2016.
6. Tavakoli, A.; Saha, S.; Arif, M.T.; Haque, M.E.; Mendis, N.; Oo, A.M.T. Impacts of grid integration of solar PV and electric vehicle on grid stability, power quality and energy economics: A review. *IET Energy Syst Integr.* **2020**, *2*, 215–225. [CrossRef]
7. Kaushal, J.; Basak, P. Power quality control based on voltage sag/swell, unbalancing, frequency, THD and power factor using artificial neural network in PV integrated AC microgrid. *Sustain. Energy Grids Netw.* **2020**, *23*, 100365. [CrossRef]
8. Radwan, A.A.; Zaki Diab, A.A.; Elsayed, A.H.M.; Alhelou, H.H.; Siano, P. Active distribution network modeling for enhancing sustainable power system performance; a case study in Egypt. *Sustainability* **2020**, *12*, 8991. [CrossRef]
9. Zapata Riveros, J.; Kubli, M.; Ulli-Beer, S. Prosumer communities as strategic allies for electric utilities: Exploring future decentralization trends in Switzerland. *Energy Res. Soc. Sci.* **2019**, *57*, 101219. [CrossRef]
10. Ramachandran, T.; Costello, Z.; Kingston, P.; Grijalva, S.; Egerstedt, M. Distributed Power Allocation in Prosumer Networks. *IFAC Proc. Vol.* **2012**, *45*, 156–161. [CrossRef]
11. Kyeremeh, F.; Fang, Z.; Yi, Y.; Peprah, F. Segmentation of a Conventional Medium Voltage Network into Solar PV Powered Microgrid. *Energy Rep.* **2023**, *9*, 5183–5195. [CrossRef]
12. Kyeremeh, F.; Fang, Z.; Liu, F.; Peprah, F. Techno-economic analysis of reactive power management in a solar PV microgrid : A case study of Sunyani to Becheam MV feeder, Ghana Branch Current to Bus Voltage Bus Injection to Branch Voltage. *Energy Rep.* **2023**, *11*, 83–96. [CrossRef]
13. Peprah, F.; Aboagye, B.; Amo-Boateng, M.; Gyamfi, S.; Effah-Donyina, E. Economic evaluation of solar PV electricity prosumption in Ghana. *Sol. Compass* **2023**, *5*, 100035. [CrossRef]
14. Gyamfi, S.; Modjinou, M.; Djordjevic, S. Improving electricity supply security in Ghana—The potential of renewable energy. *Renew. Sustain. Energy Rev.* **2015**, *43*, 1035–1045. [CrossRef]
15. Morgan, B.; Manuel, W.; Deepak, D.; Elzinga, D.; Strbac Goran Howells, M. *Smart and Just Grids: Opportunities for Sub-Saharan Africa*; Imperial College London: London, UK, 2013; pp. 1–32.
16. Sumathi, S.; Ashok Kumar, L.; Surekha, P. *Solar PV and Wind Energy Conversion Systems*; Springer International Publishing: Berlin/Heidelberg, Germany, 2015. [CrossRef]
17. Muzi, F.; Calcara, L.; Pompili, M.; Sangiovanni, S. The New Prosumer Tasks in the Energy Management of Buildings. In Proceedings of the IEEE International Conference on Environment and Electrical Engineering and Industrial and Commercial Power Systems Europe, (EEEIC/I and CPS), Palermo, Italy, 12–15 June 2018; pp. 1–4. [CrossRef]
18. Dickert, J.; Domagk, M.; Schegner, P. Benchmark low voltage distribution networks based on cluster analysis of actual grid properties. In Proceedings of the IEEE Grenoble Conference PowerTech, (POWERTECH 2013), Grenoble, France, 16–20 June 2013. [CrossRef]
19. Aboagye, B.; Gyamfi, S.; Antwi, E.; Djordjevic, S. Status of renewable energy resources for electricity supply in Ghana. *Sci. Afr.* **2021**, *11*, e00660. [CrossRef]
20. Duodu, A.; Ofosu, E.; Gyamfi, S. The Role of Solar Power in Enhancing Sustainable Energy in Electricity Generation Mix Across Ghana. *Am. Acad. Sci. Res. J. Eng. Technol. Sci.* **2022**, *88*, 292–301.

21. Karneyeva, Y.; Wüstenhagen, R. Solar feed-in tariffs in a post-grid parity world: The role of risk, investor diversity and business models. *Energy Policy* **2017**, *106*, 445–456. [CrossRef]
22. Koko, S.P. Optimal battery sizing for a grid-tied solar photovoltaic system supplying a residential load: A case study under South African solar irradiance. *Energy Rep.* **2022**, *8*, 410–418. [CrossRef]
23. Iftikhar, M.Z.; Imran, K. Network reconfiguration and integration of distributed energy resources in distribution network by novel optimization techniques. *Energy Rep.* **2024**, *12*, 3155–3179. [CrossRef]
24. Balogun, O.A.; Sun, Y.; Gbadega, P.A. Coordination of smart inverter-enabled distributed energy resources for optimal PV-BESS integration and voltage stability in modern power distribution networks: A systematic review and bibliometric analysis. *e-Prime-Adv. Electr. Eng. Electron. Energy* **2024**, *10*, 100800. [CrossRef]
25. Herding, L.; Carvalho, L.; Cossent, R.; Rivier, M. A security-aware dynamic hosting capacity approach to enhance the integration of renewable generation in distribution networks. *Int. J. Electr. Power Energy Syst.* **2024**, *161*, 110210. [CrossRef]
26. Avordeh, T.K.; Gyamfi, S.; Opoku, A.A.; Peprah, F. Assessing the viability and environmental impact of residential demand response programs: A case study in East Legon, Greater Accra, Ghana. *Energy Rep.* **2023**, *10*, 4604–4615. [CrossRef]
27. Kabir, M.N.; Mishra, Y.; Bansal, R.C. Probabilistic load flow for distribution systems with uncertain PV generation. *Appl. Energy* **2016**, *163*, 343–351. [CrossRef]
28. Leonard, L.G. *The Electric Power Engineering Handbook*, 3rd ed.; Grigsby, L.L., Harlow, J.H., McDonald, J.D., Eds.; CRC Press: Boca Raton, FL, USA, 2000. [CrossRef]
29. Augugliaro, A.; Dusonchet, L.; Favuzza, S.; Ippolito, M.G.; Sanseverino, E.R. A Backward Sweep Method for Power Flow Solution in Distribution Networks. *Electr. Power Energy Syst.* **2010**, *32*, 271–280. [CrossRef]
30. Ouali, S.; Cherkaoui, A. An Improved Backward/Forward Sweep Power Flow Method Based on a New Network Information Organization for Radial Distribution Systems. *J. Electr. Comput. Eng.* **2020**, *2020*, 5643410. [CrossRef]
31. Tortelli, O.L.; Lourenço, E.M.; Garcia, A.V.; Pal, B.C. Fast Decoupled Power Flow to Emerging Distribution Systems via Complex pu Normalization. *IEEE Trans. Power Syst.* **2014**, *30*, 1351–1358. [CrossRef]
32. Rupa, J.A.M.; Ganesh, S. Power Flow Analysis for Radial Distribution System Using Backward / Forward Sweep Method. *Int. J. Electr. Comput. Electron. Commun. Eng.* **2014**, *8*, 1540–1544.
33. Shrivastava, C.; Gupta, M.; Koshti, A. Review of Forward & Backward Sweep Method for Load Flow Analysis of Radial Distribution System. *Int. J. Adv. Res. Electr. Electron. Instrum. Eng.* **2015**, *4*, 5595–5599. [CrossRef]
34. Balaga, H.; Gupta, N.; Vishwakarma, D.N. GA trained parallel hidden layered ANN based differential protection of three phase power transformer. *Int. J. Electr. Power Energy Syst.* **2015**, *67*, 286–297. [CrossRef]
35. Wang, X.-F.; Song, Y.; Irving, M. *Modern Power Systems Analysis*; Springer US: Boston, MA, USA, 2008. [CrossRef]
36. Marini, A.; Mortazavi, S.S.; Piegari, L.; Ghazizadeh, M.S. An efficient graph-based power flow algorithm for electrical distribution systems with a comprehensive modeling of distributed generations. *Electr. Power Syst. Res.* **2019**, *170*, 229–243. [CrossRef]
37. Teng, J. Modelling distributed generations in three-phase distribution load flow. *IET Gener. Transm. Distrib.* **2008**, *2*, 330–340. [CrossRef]
38. Bolognani, S.; Zampieri, S. On the Existence and Linear Approximation of the Power Flow Solution in Power Distribution Networks. *IEEE Trans. Power Syst.* **2016**, *31*, 163–172. [CrossRef]
39. Džafić, I.; Jabr, R.A.; Neisius, H.T. Transformer Modeling for Three-Phase Distribution Network Analysis. *IEEE Trans. Power Syst.* **2015**, *30*, 2604–2611. [CrossRef]
40. Nikunj, L.; Arun, P. Forward and Backward Sweep Algorithm for Distribution Power Flow Analysis and Comparison. *Int. J. Res. Appl. Sci. Eng. Technol.* **2016**, *4*. Available online: https://www.ijraset.com/fileserve.php?FID=5957 (accessed on 27 April 2025).
41. Energy Commission of Ghana. Energy Profile of Districts in Ghana. Ghana Sustain Energy All Action Plan. 2019; pp. 25–26. Available online: https://www.energycom.gov.gh/index.php/planning/energy-district-profile (accessed on 27 April 2025).
42. Schneider Messtechnik. HT9021 DC/AC TRMS Professional Clamp Meter up to 1000A Datasheet. 2010, pp. 1–3. Available online: https://www.ics-schneider.de/wp-content/uploads/2021/05/HT9021_Datasheet_EN.pdf (accessed on 27 April 2025).

Disclaimer/Publisher's Note: The statements, opinions and data contained in all publications are solely those of the individual author(s) and contributor(s) and not of MDPI and/or the editor(s). MDPI and/or the editor(s) disclaim responsibility for any injury to people or property resulting from any ideas, methods, instructions or products referred to in the content.